

博士論文

Neurotropism and neurorestorative mechanisms in umbilical cord

derived-mesenchymal stromal cells

(臍帯由来間葉系細胞の神経向性と神経修復機序に関する検討)

向井 丈雄

## Table of contents

<b>I . Abstract .....</b>	<b>4</b>
<b>II . Abbreviations .....</b>	<b>6</b>
<b>III . Introduction .....</b>	<b>7</b>
<b>IV . Objectives.....</b>	<b>15</b>
<b>V . Materials and Methods .....</b>	<b>17</b>
<b>V -1. Isolation and culture of UC-MSCs .....</b>	17
<b>V -2. Neurogenic differentiation and neurosphere formation of UC-MSCs .....</b>	18
<b>V -3. Lentiviral vectors and UC-MSC transfection .....</b>	19
<b>V -4. <i>In vivo</i> imaging of administered UC-MSCs.....</b>	20
<b>V -5. Animal IVH model .....</b>	21
<b>V -6. Intravenous injection of UC-MSCs.....</b>	23
<b>V -7. Neurological behavioral measurement .....</b>	23
<b>V -8. Brain MRI assessment .....</b>	24
<b>V -9. Primary cultures of cortical neurons .....</b>	25
<b>V -10. Oxygen–Glucose Deprivation (OGD) of neurons and co-culture with UC-MSCs .....</b>	25
<b>V -11. Adipogenic, osteogenic, and chondrogenic differentiation of UC-MSCs .....</b>	26
<b>V -12. Flow cytometry analysis of surface markers of UC-MSCs .....</b>	27
<b>V -13. Immunocytochemistry of UC-MSCs and mouse cortical neurons .....</b>	28
<b>V -14. Immunohistochemistry of mouse brain tissue.....</b>	30
<b>V -15. Western blotting.....</b>	32
<b>V -16. Quantitative reverse transcription-polymerase chain reaction (RT-PCR).....</b>	32
<b>V -17. Migration Assays.....</b>	35
<b>V -18. TUNEL Assay .....</b>	35

<b>V-19. Fluorescent-labeled inhibitor of caspases (FLICA) labeling</b> .....	36
<b>V-20. Cortical neurons proliferation assay</b> .....	36
<b>V-21. Multiplex flow cytometry beads assay</b> .....	37
<b>V-22. Genomic DNA PCR of human Alu element</b> .....	38
<b>V-23. Statistical analysis</b> .....	39
<b>VI. Results</b> .....	<b>40</b>
<b>VI-1. Definitive markers were similar in UC-MSCs cultured with RM or MEM</b> .....	40
<b>VI-2. Neurosphere formation and neurogenic differentiation of UC-MSCs</b> .....	42
<b>VI-3. Neural marker expression in UC-MSC- and UC-MSC-neurosphere-derived cells</b> .....	44
<b>VI-4. Migration ability of UC-MSC-neurospheres</b> .....	52
<b>VI-5. IVH surgery induced ventricular dilatation evaluated by MRI</b> .....	54
<b>VI-6. UC-MSC administration improved behavioral outcome</b> .....	56
<b>VI-7. UC-MSC administration attenuated reactive gliosis resulting in the maintenance of white matter thickness in IVH mice</b> .....	59
<b>VI-8. Human-BDNF and HGF were detected only in IVH mice with UC-MSC administration</b> ....	62
<b>VI-9. Human UC-MSCs were detected in the brain and lung of IVH mice after intravenous injection</b> .....	64
<b>VI-10. Constitutive secretion of HGF and BDNF from UC-MSCs co-cultured with cortical neurons after OGD</b> .....	68
<b>VI-11. UC-MSCs restore both mature and immature neurons after OGD injury</b> .....	71
<b>VI-12. UC-MSCs support mitosis of neurons after OGD with anti-apoptotic effect</b> .....	74
<b>VII. Discussion</b> .....	<b>79</b>
<b>VIII. References</b> .....	<b>99</b>
<b>IX. Acknowledgments</b> .....	<b>117</b>

## **I. Abstract**

Neonatal encephalopathy during the perinatal period is the cause of cerebral palsy that doesn't have fundamental treatments once it has manifested. Recent advances of regenerative cell therapies give us encouraging expectations in treating cerebral palsy. Here I focused on umbilical cord-derived mesenchymal stromal cells (UC-MSCs) as a new treatment tool for suppressing the onset of cerebral palsy, and aimed to investigate the effectiveness and mechanisms of UC-MSCs for neonatal brain injuries.

In the study, I demonstrated UC-MSCs have neurogenic differentiation potential and migration ability towards injured neuronal cells *in vitro*. Next, I established neonatal intraventricular hemorrhage (IVH) mice model, one of neonatal brain injuries and found that the intravenous injection of UC-MSCs improved behavioral outcome in IVH, by restoring periventricular reactive gliosis, hypomyelination, and periventricular cell death *in vivo*.

Transplanted UC-MSCs migrated towards injured brain, but disappeared three weeks after injection. Interestingly, human brain-derived neurotrophic factor (BDNF) and hepatocyte growth factor (HGF) were elevated in the serum, cerebrospinal fluid and brain tissue of UC-MSCs injected mice. The BDNF and HGF secreted from UC-MSCs were functional in restoring injured primary fetal neurons by retaining neurites and anti-apoptosis, while these effects were attenuated by inhibition of them *in vitro*.

These results suggest that UC-MSCs ameliorate neuronal injury followed by functional improvement by secretion of neurotrophic factors such as BDNF and HGF rather than neuronal differentiation and eternal cell replacement, and that intravenous injection of UC-MSCs may be feasible treatment for neonatal brain injuries.

## **II. Abbreviations**

UC, umbilical cord

MSCs, mesenchymal stromal cells

IVH, intraventricular hemorrhage

BM, bone marrow

BBB, blood brain barrier

CSF, cerebrospinal fluid

MAP2, microtubule-associated protein 2

GFAP, glial fibrillary acidic protein

PAX6, paired box 6

OCT4, octamer-binding transcription factor 4

KLF4, Kruppel-like factor 4

MBP, myelin basic protein

GAPDH, glyceraldehyde 3-phosphate dehydrogenase

TUNEL, terminal deoxynucleotidyl transferase-mediated dUTP nick-end labeling

BDNF, brain-derived neurotrophic factor

NGF, nerve growth factor

HGF, hepatocyte growth factor

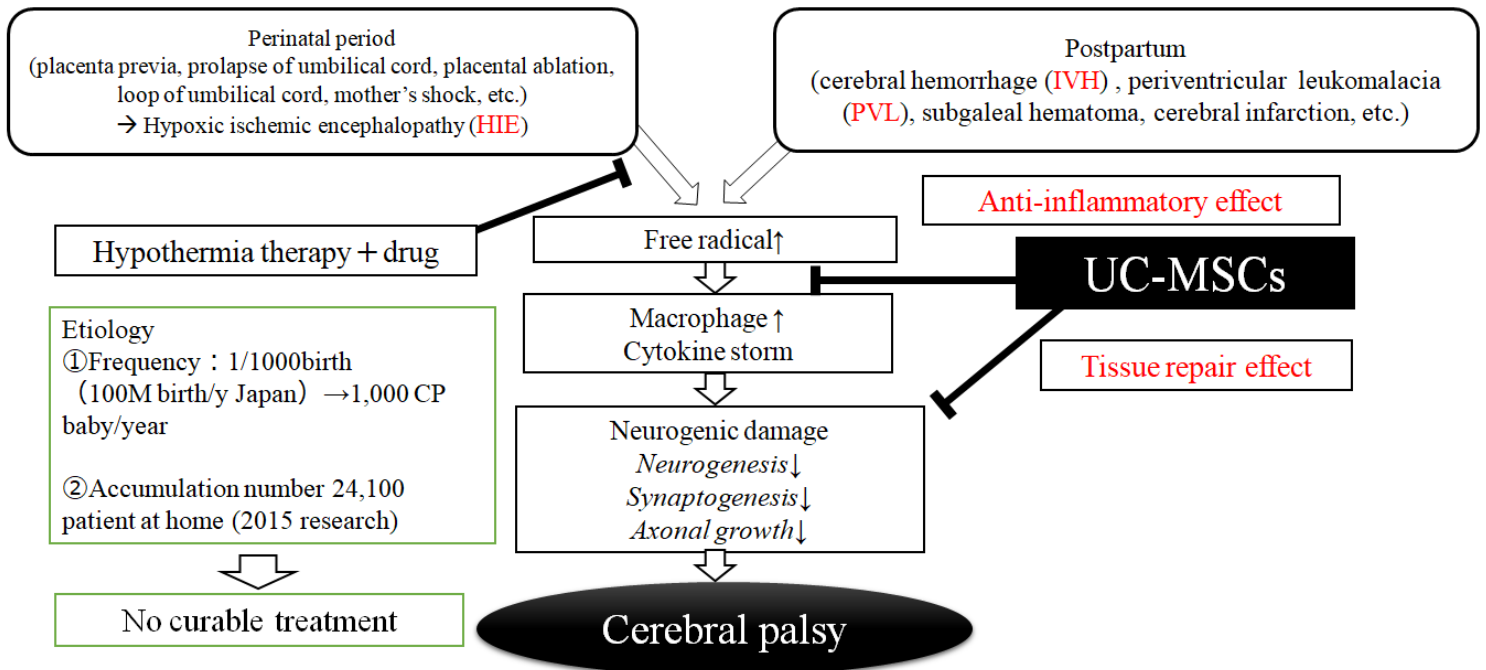
OGD, oxygen glucose depletion

### **III. Introduction**

Neonatal brain damage during the perinatal period is the cause of cerebral palsy later in life, and is a condition which places a great burden on not only the infant but also the family who raises. Those who present central nervous symptoms such as consciousness disorder, breathing / nursing disorder and spasms etc. in the neonatal period are collectively referred to as having "neonatal encephalopathy", and this is a condition that is by no means rare, and is incident in approximately 1-2 people per 1000 births in Japan. Perinatal brain damage that causes cerebral palsy includes (1) Hypoxic-ischemic encephalopathy (HIE), (2) Intraventricular hemorrhage (IVH), (3) Periventricular leukomalacia (PVL) etc., and the main pathological condition is an increase in active oxygen species rise resulting from mitochondrial dysfunction, macrophage activation as well as acute inflammation called high cytokineinemia which accompanies all of these.[1].

There are expectations for cell therapies with neuroprotective action accompanied by neurotrophic factor secretions for neonatal encephalopathy that do not have effective treatments once they have manifested. I focused on the anti-inflammatory effect and tissue repair ability of umbilical cord-derived mesenchymal cells (UC-MSCs) as a new treatment for suppressing the onset of cerebral palsy (Figure 1).

**Figure 1. The process leading to cerebral palsy of neonatal encephalopathy and adaptation of UC-MSCs (Modified from reference [2])**



In addition to their own ability to differentiate, MSCs have the ability to migrate to inflammatory sites and tissues, and also has inflammation suppressing action, immunomodulatory ability and tissue repairing ability associated with it. MSCs can also be obtained from various tissues other than the umbilical cord (bone marrow, umbilical cord blood, adipose tissue, placenta etc.), and clinical research has already been conducted on bone marrow-derived MSCs as a therapeutic drug for neuropathies like spinal cord injury[3].

Among several sources, UC-MSCs are: (1) not physically invasive for the donor and have no ethical issues, because the umbilical cord, which is the source of the cells, has been discarded as medical waste; (2) easy to sample, store and transport because they are an abundant source associated with childbirth; (3) have pluripotency to various tissue cells including the nervous system; (4) thought to be useful as a cell therapy for cerebral palsy because they have low immunogenicity while having sufficient immunosuppressive ability[4].

While having an inflammation inhibitory effect inducing inflammation-suppressing substances like indoleamine 2,3-dioxygenase (IDO) during inflammation [5], at the same time UC-MSCs are said to be able to differentiate into neural stem cells, and the presence of neurotrophic factors which promote nerve regeneration has also been suggested[6, 7]. These effects are thought to be very effective against neonatal brain disorders in which inflammation and neuropathy are the primary conditions. Even in animal experiments, UC-MSCs have been reported to be useful for treating nervous system disorders[8, 9]. In addition, many clinical

trials using UC-MSCs have been conducted for the purpose of immunomodulatory, anti-inflammatory and tissue repair (Table 1). Among them, clinical studies on cranial nervous system disorders have already been conducted, and the target diseases include spinocerebellar degeneration, spinal cord injury, traumatic encephalopathy, cerebral palsy in adolescence and early adulthood.

Based on the above, by clarifying the usefulness of UC-MSCs and its mechanism of action as a subject for neonatal encephalopathy, it was thought that novel cell therapy using UC-MSCs is effective in preventing the onset of cerebral palsy and lead to the improvement of QOL for children with cerebral palsy, as well as their families.

In clinical trials, intrathecal injection is often used as a route of administration in neurogenic disorders. However intrathecal injection and intraventricular injection may have some risk over intravenous injection for neonates with neonatal encephalopathy. Whether intravenously injected UC-MSCs can migrate to the injured brain area and attenuate neuronal injury such as periventricular reactive gliosis and hypomyelination after neonatal IVH has not yet been investigated, and the mechanisms underlying the effects of UC-MSC treatment on such neuronal injury remain unknown. In addition, because supplemented fetal bovine serum (FBS) in the medium with which UC-MSCs are cultured introduces the possibility of xenogeneic antigens and infections including bovine spongiform encephalopathy (BSE), lower antigenic and safer medium is needed for clinical use. Therefore, in this study, I used

the serum-free new medium, RM medium, for the culture of UC-MSCs for clinical use as an alternative to FBS containing  $\alpha$ -MEM medium, and I investigated the restorative effect of UC-MSCs cultured with RM medium and the mechanisms of them in a neonatal brain injured model.

**Table1. Clinical trial using UC-MSCs (Modified from reference [4])**

Reference	Disease	Number of patients	Mean age (range), year	Route	Dose	Number of treatments	Results	Adverse events
Wu <i>et al.</i> [10] (2011)	Severe steroid-resistant aGVHD	2	Case 1: 4	IV	3.3, 7.2, 8.0 $\times 10^6$ /kg	3	Improved bilirubin level and diarrhea	No
			Case 2: 6	IV	4.1 $\times 10^6$ /kg	1		
Fu <i>et al.</i> [11] (2013)	Refractory severe AA	5	15.2 (9-22)	IV (2 days after PBSCT)	1 $\times 10^6$ /kg	1	No severe aGVHD or cGVHD	No
Wang <i>et al.</i> [12] (2013)	Severe AA	22	18.83 (3-52)	IV with HSCT	1.2 $\times 10^6$ /kg	1	Rapid engraftment, 7/22 aGVHD I-II	No
Si <i>et al.</i> [13] (2014)	Severe aplastic anemia	37	5.00 (0.75-11.58)	IV (7-10 days after HSCT)	1 $\times 10^6$ /kg	1	Engraftment, aGVHD II-IV: 17 of 37 (45.9%) cGVHD: 7 of 37 (18.9%)	No
Wu <i>et al.</i> [14] (2013)	Refractory/relapsed hematologic malignancy	50	26 (9-58)	IV (4 hours before haploidentical HSCT)	5 $\times 10^5$ /kg	1	Engraftment, aGVHD II-IV: 12 of 50 (24.0%) cGVHD: 17 of 45 (37.7%) (3 extended)	No
Zhu <i>et al.</i> [15] (2015)	High-risk acute leukemia	25	11.2 (4-17)	IV (before haploidentical HSCT)	Median 1.14 $\times 10^6$ /kg at 7-day intervals	4	aGVHDI: 8 of 25 (32.0%) cytomegalovirus viremia: 23 of 25 (92.0%)	No

**Table1 (continued)**

Reference	Disease	Number of patients	Mean age (range), year	Route	Dose	Number of treatments	Results	Adverse events
Dongmei <i>et al.</i> [16] (2011)	SCA/MSA-C	14/10	46	IT	$1 \times 10^6$ /kg at 7-day interval	4	Delayed progression of neurological deficits	Dizziness, back pain, headache
Jin <i>et al.</i> [17] (2013)	Hereditary SCA	16	39.9 (21-56)	IV + IT	IV: $4 \times 10^7$ IT: $2 \times 10^7$ cells at 7-day interval	4	Motor functional recovery after 6 Mm	No
Wang <i>et al.</i> [18] (2013)	Traumatic brain injury	20	27.5 (5-48)	IT	$1 \times 10^7$ at 5-7 day interval	4	Motor functional recovery after 6 Mm	No
Wang <i>et al.</i> [19] (2015)	Cerebral palsy	16 (8 twins)	6.29 (3-12)	IT	$1 \sim 1.5 \times 10^7$ cells at 3-5 day interval	4	Motor functional recovery after 1 & 6 months	No
Li <i>et al.</i> [20] (2015)	Coronary chronic total occlusion	15	unknown	Intracoronary injection	$3, 4, 5 \times 10^6$ /kg	1	Infarcted size reduced with improved left ventricular ejection fraction.	No
Zhao <i>et al.</i> [21] (2015)	Severe systolic heart failure	30	52.9 (20-79)	Intracoronary injection	unknown	1	Cardiac remodeling and function improved with reduced mortality rate	No
Musialek <i>et al.</i> [22] (2015)	Acute myocardial infarction	10	55.6 (32-65)	Intracoronary injection	$3 \times 10^7$ /body	1	Feasible and safe as off-the-shelf cellular therapy	Transient fever (38.9 °C)
Can <i>et al.</i> [23] (2015)	Myocardial ischemia	39	30-80	Intracoronary injection	$2 \times 10^7$ /kg	1	On going	No
Shi <i>et al.</i> [24] (2012)	Acute-on-chronic liver failure	24	40 (24-59)	IV	$0.5 \times 10^6$ /kg at 4-week interval	3	Improved survival rate and partial liver function	No

**Table1 (continued)**

Reference	Disease	Number of patients	Mean age (range), year	Route	Dose	Number of treatments	Results	Adverse events
Xue <i>et al.</i> [25] (2015)	Decompensated liver cirrhosis	50	unknown	Intrahepatic artery injection	$3 \times 10^7$ /body	1	Serum pre/albumin increased 24 weeks post surgery	No
Wang <i>et al.</i> [17] (2013)	Primary biliary cirrhosis	7	49 (33-58)	IV	$5 \times 10^5$ /kg at 4-week interval	3	ALP and $\gamma$ -GTP decreased	No
Cai <i>et al.</i> [26] (2014)	Avascular necrosis of the femoral head	30	41.6 (19-63)	Femoral head artery (co-transplant with autologous BM)	Autologous BM-MN Cs: $60.7 \pm 11.5 (\times 10^6 / \text{kg})$ UC-MSCs: $1 \times 10^6 / \text{kg}$	1	Improved symptoms	No
Guan <i>et al.</i> [27] (2011)	DM type 2	6	40.5 (27-51)	IV	$1 \times 10^6$ /kg at 2-week interval	2	Three patients became insulin-independent between 25 and 43 months	No
Wang <i>et al.</i> [28] (2014)	Active and refractory SLE	40	17-54	IV	$1 \times 10^6$ /kg on day 0 and day 7	2	MCR (32.5%) and PCR (27.5%) during 12 months, although several patients relapsed after 6 months	No

IV, intravenous injection; aGVHD, acute graft-versus-host- disease; HSCT, hematopoietic stem cell transplantation; BM, bone marrow; SCA, spinocerebellar ataxia; MSA-C, multiple system atrophy-cerebellar type; IV, intravenous injection; IT, intrathecal injection; DM, diabetes mellitus; SLE, systemic lupus erythematosus; RA, rheumatoid arthritis; ALP, alkaline phosphatase; MCR, major clinical response; PCR, partial clinical response

## **IV. Objectives**

Clarifying the usefulness of UC-MSCs and its mechanism of action for neonatal encephalopathy leads to novel cell therapy using UC-MSCs in preventing the onset of cerebral palsy and lead to the improvement of QOL for children with cerebral palsy, as well as their families. Therefore I focused on the following two items in this research.

### **IV-1. Neurotropism of UC-MSCs**

I examined the neural tropism, such as whether UC-MSCs have neural specific markers expression, neural differentiation ability, neurosphere-forming ability, and whether neurotrophic factors are secreted from UC-MSCs. I also examined whether UC-MSCs have migratory ability towards damaged cells using *in vitro* damaged neuronal cell model.

### **IV-2. Neurorestorative effect and mechanisms of UC-MSCs in a neonatal brain injury model**

If neurotropism of UC-MSCs is observed, then UC-MSCs cultured with  $\alpha$ -MEM medium containing 10% FBS or with serum-free new medium, RM medium, are administered to neonatal brain injury model *in vivo*, and behavioral function is examined accompanied by pathological analysis. Furthermore, I examined whether the behavioral and pathological changes are caused by neuronal differentiation and cell replacement by UC-MSCs, or are caused by neurotrophic factors secreted from UC-MSCs. Finally I proved these mechanisms

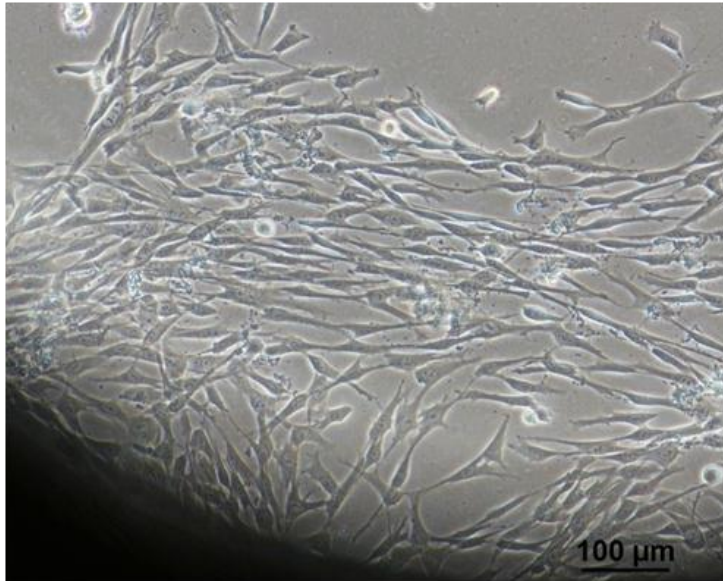
*in vitro* using primary culture of fetal mouse neurons.

## **V. Materials and Methods**

### **V-1. Isolation and culture of UC-MSCs**

The present study was approved by the Ethics Committee of the Institute of Medical Science, University of Tokyo, Yamaguchi Hospital and the NTT Medical Center Hospital, Japan. UCs were collected after informed consent was obtained from pregnant women planning to undergo cesarean sections. The fresh and frozen-thawed UC tissues were minced into 1–2 mm<sup>3</sup> fragments with Cellamigo® (Tsubakimoto Co., Japan) for improved explant isolation[29]. Tissue fragments were cultured with  $\alpha$ MEM (MEM; Wako Pure Chemical Industries, Ltd., Japan) supplemented with 10% FBS and antibiotics-antimycotics (Antibiotic-Antimycotic, 100X; Life Technologies, USA) or RM medium (RM; kindly provided by ROHTO Pharmaceutical Co., Ltd., Japan), which is a serum-free culture medium at 37°C with 5% CO<sub>2</sub>. The fibroblast-like adherent cells begin to migrate from the tissue fragments (Figure 2) and they were harvested using TrypLE Select (Life Technologies), and the fragments removed by filtering with a 100- $\mu$ m cell strainer. These cells were defined as passage 1 (P1) cells. UC-MSCs were cryopreserved in cryoprotectant, STEM-CELLBANKER (ZENOAQ Resource Co, Ltd.) and thawed just before use. UC-MSCs used in each experiment were derived from the same umbilical cord donor, and the experiments were performed repeatedly with MSCs derived from different umbilical cords.

**Figure2. UC-MSCs erupted from umbilical cord**



## **V-2. Neurogenic differentiation and neurosphere formation of UC-MSCs**

UC-MSCs were plated at a density of  $4 \times 10^3$  cells/cm<sup>2</sup> in 24 well plate (BD Falcon, USA) with MEM with 10% FBS, and cultured until 80–90% confluency. UC-MSCs were rinsed with phosphate-buffered saline (PBS), induced with MSC Neurogenic Differentiation Medium (PromoCell GmbH, Germany), and incubated for at least 3 days, with the medium being changed every 2 days.

As for neurosphere formation, UC-MSCs were plated at a density of  $1 \times 10^4$  cells/well in 96-well Nunclon™ Sphera™ Microplates (Thermo Fisher Scientific Inc, USA) using DMEM/F12 medium (Wako Pure Chemical Industries, Ltd., Japan) supplemented with 20 ng/mL of epidermal growth factor (EGF, Sigma-Aldrich, Japan), 20 ng/mL of basic

fibroblast growth factor (bFGF, Sigma-Aldrich, Japan), and antibiotics-antimycotics. Medium was changed every 2 days for 3–7 days to generate neurospheres. For neurogenic differentiation, the formed spheres were transferred to 24-well plates (BD Falcon, USA), allowed to adhere, cultured with MSC Neurogenic Differentiation Medium (PromoCell GmbH; PromoCell, Germany), and incubated for at least 3 days, with medium changes every 2 days. Some spheres were used for immunostaining or RNA extraction, and the remaining ones were dissociated using Accutase (Innovative Cell Technologies, Inc., USA) for cell counting, cell viability testing, and migration assays. Briefly, neurospheres were transferred to a 15 mL conical tube, and centrifuged at 100 g for 1 min. The supernatant was discarded and 1 mL of Accutase was added to the pelleted spheroids, and incubated at room temperature for 10 min. Neurospheres were then dissociated by pipetting to form a single cell suspension prior to cell quantitation by Trypan blue exclusion assay.

Therefore following experiments of neurogenic differentiation *in vitro* were performed among four groups: (1) undifferentiated UC-MSCs, (2) differentiated UC-MSCs, (3) undifferentiated UC-MSC-neurospheres, and (4) differentiated UC-MSC-neurospheres.

### **V-3. Lentiviral vectors and UC-MSC transfection**

The third generation lentiviral vector system was used to transduce UC-MSCs with firefly luciferase gene (Fluc) for *in vivo* monitoring of xenogeneic UC-MSC migration and

with green fluorescent protein (GFP) for cell sorting and in vitro detection of UC-MSCs. The transfer vector CSII-EF-Fluc-2A-EGFP was transfected into 293T cells together with pCAG-HIVg/p.PRE, pCMV-VSV-G-RSV-rev, and pMDG. After 48 hours post-transfection, virus-containing supernatant was harvested by collecting the medium, and high titer viral vectors were prepared as previously reported [30]. UC-MSCs were cultured, and when the culture reached 80% confluence, the concentrated lentivirus was added to the culture dishes. After incubation for 48 hours, the medium was replaced with conditioned medium. Then cells were sorted according to their GFP fluorescence using a BD FACS Aria (BD Biosciences).

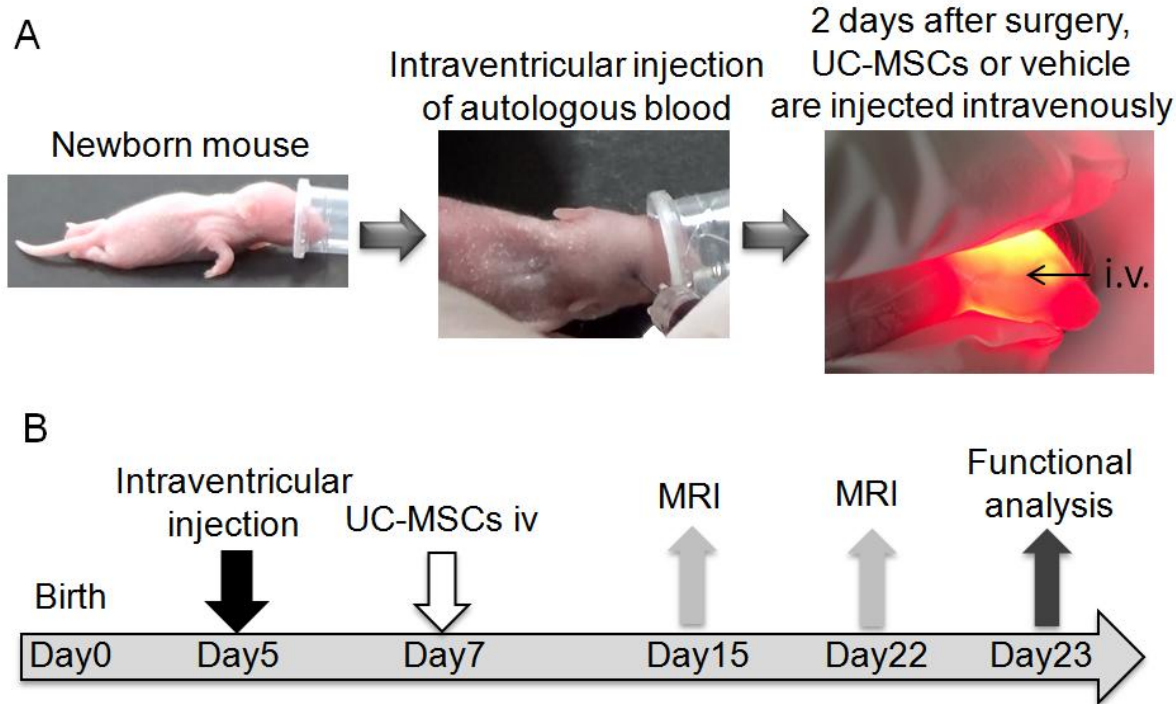
#### **V-4. *In vivo* imaging of administered UC-MSCs**

For UC-MSC *in vivo* imaging, mice were examined at different time points after UC-MSC administration using the imaging system IVIS 100 (Xenogen Corporation). The luminescent signals from the mice were traced at the indicated time points after intravenous administration of UC-MSCs using the *in vivo* imaging system. D-Luciferin dissolved in PBS was given to each mouse by intraperitoneal injection at a dose of 150 mg/kg, and the mice were left for 15 min followed by anesthesia in a chamber by isoflurane inhalation. Mice were then imaged with an exposure time of 5 min, and photographic images were analyzed using the Living Image software.

## **V-5. Animal IVH model**

All experimental procedures were approved by the Animal Experiment Committee of the Institute of Medical Science, The University of Tokyo and were done according to the institutional ethical guidelines for animal experiments. Newborn postnatal day 5 (P5) B6 Albino mice (B6N-Tyrc-Brd/BrdCrCrI, Charles River Laboratories International, Inc.) were used for the experiments (n = 86). Mice pups of both sexes were used. They were randomly assigned to the experimental groups. Figure 3A shows the experimental design. The mice were anesthetized with isoflurane (3% for induction and 1-2% for maintenance) in oxygen-enriched air, and maternal whole blood (20  $\mu$ l) collected in a sterile syringe was infused slowly into the right ventricle as previously reported [31]. Because the neonate mice could not be placed in a stereotaxic frame, the injections of blood were done freehand with the needle inserted percutaneously as previously reported [31]. The needle was introduced into the right periventricular region of the mouse (approximately 0.5 mm posterior and 1.0 mm lateral of the right eye and 3.0 mm deep from the scalp surface). Blood was injected slowly over 1 min, and the needle was kept in place for 10-20 s and then removed slowly. After the procedure, mice were returned to their dams. Brain magnetic resonance imaging (MRI) was performed at P6 in order to confirm the extent of IVH, and mice with similar degrees of IVH were included in following experiments. All mice were weighed regularly and were euthanized by CO<sub>2</sub> asphyxiation at P23.

**Figure3. Experimental protocol of neonatal model of intraventricular hemorrhage and UC-MSCs administration**



(A) At postnatal day 5 (P5), 20µl of dam’s blood was introduced into the right periventricular region of mouse brain under anesthesia. After confirming severe IVH by brain MRI, mice were administered frozen-thawed UC-MSCs at  $1 \times 10^5$  in 20 µl cryoprotectant, or cryoprotectant alone, intravenously via the superficial temporal vein at P7 (2 days after IVH surgery). (B) Experimental protocol scheme. Brain MRI was performed at P15 and P22 after IVH procedure, and neurological behavioral measurements were performed at P23.

## **V-6. Intravenous injection of UC-MSCs**

After confirming severe IVH by brain MRI at P6, mice were administered frozen-thawed UC-MSCs at  $1 \times 10^5$  in 20  $\mu$ l cryoprotectant, or cryoprotectant alone, intravenously via the superficial temporal vein [32] at P7 (2 days after IVH surgery). The mice were divided into four groups: IVH with  $\alpha$ MEM medium-cultured UC-MSC administration (IVH + UC-MSCs (MEM); n=13); IVH with RM-cultured UC-MSC administration (IVH + UC-MSCs (RM); n=36); IVH with vehicle injection (IVH; n=20); or normal control (Control; n=17), respectively. All mice tolerated the IVH procedure, and there was no surgical mortality.

## **V-7. Neurological behavioral measurement**

Open field test and footprint analysis were performed on P23 (Figure 3B). An open field box consisted of a square of 40×40 cm surrounded by a 35 cm wall square box, and each mouse was placed in the box and allowed to explore for ten minutes. Overall activity in the box was recorded with a video monitor, and the distance traveled and number of times rearing were measured to assess locomotor activity and anxiety. In the footprint analysis, a semi-circle pipe (35 mm diameter, 375 mm lengthwise) was placed on a white paper. Each mouse had its paws covered in nontoxic paints (forepaws in green and hind paws in red). The mice were allowed to walk from one end of the pipe. Three trials were performed, paw prints

were scanned using a scanner, and two to four steps of each run were measured for (i) hind-stride length, (ii) hind-base width (the distance between the right and left hind limb strides), and (iii) hind-base angle difference (the difference in angle from the median line between right and left hind-base) [33] to assess motor coordination and synchrony with or without limb paralysis. Both behavioral experiments were performed by an individual who was blinded to the treatment.

#### **V-8. Brain MRI assessment**

Brain MRI was performed using a Bruker ICON 1-T MRI system (Bruker BioSpin Corp., Billerica, USA) at P15 and P22 (Figure 3B). Sedation was achieved with 1.5–2% isoflurane, and heart and respiratory rates were monitored during MRI imaging. T2-weighted MRI was performed with the following parameters: echo time = 85 ms, repetition time = 2,800 ms, field of view =  $20 \times 20 \text{ mm}^2$ , matrix size of  $128 \times 128$ , and total 11 slices with slice thickness 0.8 mm. The total volume proportion was calculated using ParaVision software (version 6.0, Bruker) as previously described [34]. One MRI session was approximately 20 min on average per mouse, and after MRI imaging, the mice were allowed to recover and were returned to their dams.

## **V-9. Primary cultures of cortical neurons**

All experiments were carried out in accordance with the Animal Experiment Committee of the Institute of Medical Science, The University of Tokyo. Cortical neurons from B6 Albino mice (B6N-Tyrc-Brd/BrdCrCrI, Charles River Laboratories International, Inc.) were prepared according to previous reports [35, 36]. Briefly, pregnant 16 days old mice were euthanized, and fetus were taken in sterile conditions. Fetal brains were removed and cortical tissues were dissected under microscope. Meninges were removed and cortical tissue were chopped into small pieces. Cells were dispersed followed by mechanical trituration using Neuron Dissociation Solutions (Wako Pure Chemical Industries, Ltd., Japan) and filtered through a 70 $\mu$ m pore-size cell strainer. The cells were resuspended in the neurobasal medium (GIBCO) supplemented with 2% B27 (Invitrogen) and plated onto Poly-L-Lysine Culture Dishes (BioCoat™, Corning Inc. Japan) coated plates. Cells were cultured in a humidified incubator at 37°C with 5% CO<sub>2</sub>, and half of the medium was replaced with fresh medium every three days. To reduce contamination with glial cells, 10  $\mu$ M cytosine arabinofuranoside (Sigma-Aldrich) was added for 24 h at DIV 4.

## **V-10. Oxygen–Glucose Deprivation (OGD) of neurons and co-culture with UC-MSCs**

OGD model was established as previously described [35, 37]. For deprivation of glucose primary cortical neurons were washed twice with phosphate buffered saline and

cultured in glucose-free DMEM (GIBCO). In addition, cells were incubated in an anaerobic chamber (95% N<sub>2</sub>, 5% CO<sub>2</sub>) at 37°C. The OGD condition was maintained for 4 h, after which cells were re-oxygenated in the original medium and placed in a normoxic chamber (37°C, 5% CO<sub>2</sub>). Neurons were co-cultured with UC-MSCs as previously reported [38]. Briefly using a 24-well Transwell chamber (Corning, USA) equipped with an 8- $\mu$ m filter membrane, cortical neurons were cultured in the bottom chamber, while in the upper chamber, UC-MSCs were plated at  $5 \times 10^4$  cells/well and co-cultured overnight at 37 °C with 5% CO<sub>2</sub>. In the experiment of HGF and BDNF concentration measurement in the culture supernatant,  $\alpha$ MEM without FBS in culturing UC-MSCs was used during co-culture.

#### **V-11. Adipogenic, osteogenic, and chondrogenic differentiation of UC-MSCs**

UC-MSCs were plated at a density of  $2 \times 10^4$  cells/well in 12-well plates, and induced to differentiate into adipocytes with culture medium supplemented with 100  $\mu$ M indomethacin (Sigma-Aldrich, Japan), 0.5 mM 3-isobutyl-1-methylxanthine (Sigma-Aldrich, Japan), and 10  $\mu$ g/mL insulin (Sigma-Aldrich, Japan) [39]. We performed adipogenic differentiation by treating the UC-MSCs with cocktail medium for 3 weeks, and the medium was replenished every 3 days, followed by staining with Oil Red O (Sigma-Aldrich, Japan) to detect lipids.

To investigate the osteogenic differentiation capacity of UC-MSCs, cells were cultured in 24-well plates in MEM supplemented with 10% FBS. On the following day, the medium was replaced with osteogenic induction medium containing 10 nM dexamethasone (Sigma-Aldrich, Japan), 10 mM  $\beta$ -glycerol phosphate (Sigma-Aldrich, Japan), 100 mM ascorbic acid (Sigma-Aldrich, Japan), and 50 ng/mL recombinant human bone morphogenic protein 2 (rhBMP2; Peprotech, USA)[40]. The induction medium was replenished every 3 days. After 1-2 weeks, the cells were stained with an alkaline phosphatase staining kit (Sigma-Aldrich, Japan), rinsed with water, and examined by microscopy.

A pellet culture system in chondrogenic differentiation was used to evaluate the capacity of UC-MSCs to differentiate to chondrocytes. For this,  $2.5 \times 10^5$  pelleted UC-MSCs were resuspended and cultured in Stem MACS™ ChondroDiff Media (Miltenyi Biotec, Inc., Germany) in 15 mL conical tubes with medium changes every 3 days. After 3 weeks in culture, the pellet was fixed with 4% formaldehyde, sliced, and stained with 0.05% toluidine blue (Sigma-Aldrich, Japan) to detect extracellular matrix by metachromasia.

## **V-12. Flow cytometry analysis of surface markers of UC-MSCs**

Standard flow cytometry techniques were used to determine the presence of MSC markers as described elsewhere [41]. UC-MSCs were stained using the Human MSC Analysis kit (BD Biosciences, USA) containing the following mouse monoclonal antibodies (mAbs):

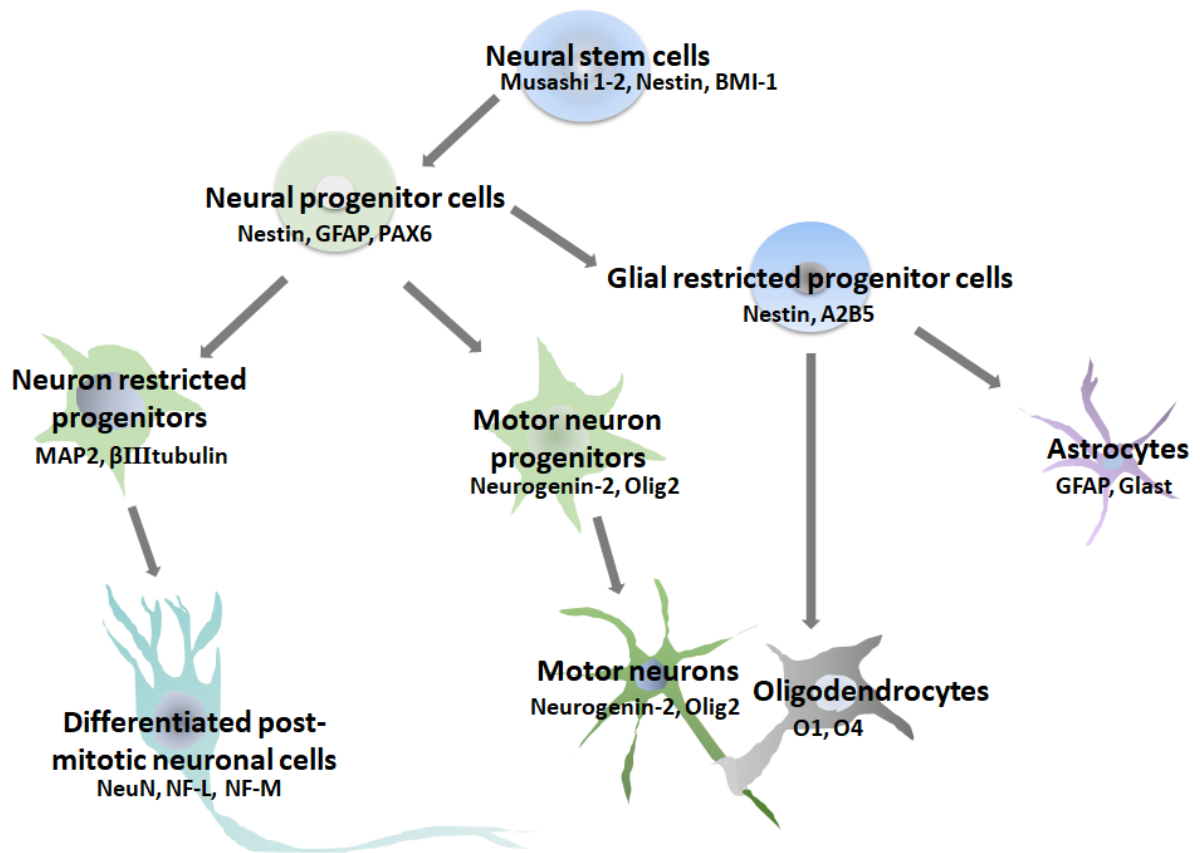
fluorescein isothiocyanate (FITC)-conjugated anti-human CD90; phycoerythrin (PE)-conjugated anti-human CD105; allophycocyanin (APC)-conjugated anti-human CD73; and FITC-, PE-, and APC-conjugated anti-mouse IgG isotype controls (BD Biosciences). Alternatively, UC-MSCs were stained with FITC-conjugated anti-HLA-DR (BD Biosciences), FITC-conjugated anti-human CD44 (BD Biosciences), FITC-conjugated anti-human CD34 (BD Biosciences), PE-conjugated anti-human CD 11b (BD Biosciences), PE-conjugated anti-human CD 19 (BD Biosciences), PE-conjugated anti-HLA-ABC (BD Biosciences) or APC-conjugated anti-CD45 (BD Biosciences). Propidium iodide was used to identify and exclude dead cells by flow cytometry.

### **V-13. Immunocytochemistry of UC-MSCs and mouse cortical neurons**

The expression of neural protein markers was analyzed by immunocytochemistry. A scheme of neuronal differentiation and the expression of major neural markers is shown in the Figure 4. Briefly, the cells were fixed with 4% paraformaldehyde for 30 min at room temperature, blocked with PBS containing 10% normal donkey serum (Sigma-Aldrich, Japan) and 0.3% Triton-X 100 (Sigma-Aldrich, USA), followed by overnight incubation with primary antibodies at 4°C. The primary antibodies included mouse anti-human microtubule-associated protein 2 (MAP-2; 1:200 dilution, Abcam), rabbit anti-human  $\beta$ III-tubulin (1:200, Abcam), rabbit anti-human glial fibrillary acidic protein (GFAP; 1:1000

dilution, Abcam), mouse anti-human Nestin (1:1000 dilution, BioLegend), mouse anti-human PAX6 (1:200 dilution, Santa Cruz Biotechnology), rabbit anti-human Nanog (1:100 dilution, ReproCELL), mouse anti-human KLF4 (1:1000 dilution, Abcam), goat anti-human oct3/4 (10 µg/ml, R&D Systems), rabbit anti-human MUSASH1 (1:200, Abcam) rabbit, anti-growth associated protein-43 (GAP-43; 1:500 dilution, Abcam), and mouse anti- Histone H3 (1:500 dilution, Abcam). Secondary antibodies used were donkey anti-mouse IgG heavy and light chain-specific (H&L) (Alexa Fluor® 488) (1:1000; Abcam), donkey anti-rabbit IgG H&L (Alexa Fluor® 594) (1:1000; Abcam), and donkey anti-goat IgG NorthernLights™ NL557-conjugated antibody (1/1000, R&D Systems). Nuclei were counterstained with 4',6-diamidino-2-phenylindole (DAPI; Sigma-Aldrich, Japan), and images were acquired using a fluorescence microscope (Nikon Eclipse Ti, Nikon Instruments Inc., Japan) and NIS-Elements microscope imaging software version 4.10. To objectively enumerate Histone H3-positive cells, Image J software version 1.49 was used. The positive cells were counted in 5 randomly-selected fields at a magnification of 200x using a microscope (Nikon Eclipse Ti, Nikon Instruments Inc., Japan), and the proportion of positive cells was calculated as number of Histone 3-positive cells/total number of cells × 100%.

**Figure4. Neural differentiation and neural markers**



#### **V-14. Immunohistochemistry of mouse brain tissue**

The brains were removed from the mice after euthanasia at P23 and fixed overnight with 4% paraformaldehyde at room temperature. Fixed brains were embedded in paraffin, and sectioned coronally at the level of 1 mm anterior to 0.5 mm posterior of bregma. Three coronal sections per mouse were obtained, and five random non-overlapping fields were assessed from each section [42]. Briefly, paraffin sections were deparaffinized, rehydrated, and blocked with PBS containing 10% normal donkey serum (Sigma-Aldrich, Japan) and

0.3% Triton-X 100 (Sigma-Aldrich, USA), followed by overnight incubation with primary antibodies at 4 °C. The primary antibodies included anti-human/mouse MAP2 (microtubule-associated protein 2; 1:200 dilution, Abcam), anti-human/mouse GFAP (glial fibrillary acidic protein; 1:200, Abcam), anti-HLA Class 1 (1:1000, Abcam), and anti-human CD105 (1:900, Abcam). Secondary antibodies were donkey anti-mouse IgG heavy and light chain-specific (H&L; Alexa Fluor® 488; 1:1000; Abcam) and donkey anti-rabbit IgG H&L (Alexa Fluor® 594; 1:1000; Abcam). Nuclei were counterstained with DAPI (4',6-diamidino-2-phenylindole; Sigma-Aldrich, Japan). For myelin basic protein (MBP) staining, after deparaffinization, rehydration, and serum blocking, sections were incubated overnight at 4 °C with goat anti-human/mouse MBP antibody (1:200 dilution, Santa Cruz Biotechnology, USA). Sections were washed and then incubated with donkey anti-goat IgG horseradish peroxidase (HRP) and donkey anti-rabbit IgG HRP (1:5,000, Santa Cruz Biotechnology, USA), respectively. Sections were finally stained with 3,3'-diamino benzidine (DAB). Images were acquired using a fluorescence microscope (Nikon Eclipse Ti, Nikon Instruments Inc., Japan) and NIS-Elements microscope imaging software version 4.10. I averaged the numbers of immunoreactive cells from 15 randomly selected periventricular locations per mouse (5 fields per section × 3 sections per mouse; n = 3 mice per group) using ImageJ software, as previously described [43].

### **V-15. Western blotting**

Proteins were extracted from the cells according to the manufacturer instructions. Protein concentrations of the samples were measured using the RC DC Protein Assay kit (Bio-Rad) and equal amounts of the protein and sample loading buffer were boiled for 5 min and separated by sodium dodecylsulfate polyacrylamide gel electrophoresis (SDS-PAGE), followed by transfer onto PVDF membranes (Immobilon-P Membrane, PVDF, Millipore). The membranes were blocked with 5% skim milk in Tris, sodium chloride, and Tween 20 (TNT) buffer and incubated overnight at 4°C with the primary antibodies indicated above, and anti-beta-tubulin (Wako Pure Chemical Industries, Ltd., Japan) at the recommended dilutions. This was followed by incubation with secondary antibodies (horseradish peroxidase-conjugated anti-goat IgG, horseradish peroxidase-conjugated anti-rabbit IgG, horseradish peroxidase-conjugated anti-mouse IgG) for 1 h at room temperature. PVDF membranes were visualized using an enhanced chemiluminescence system with Pierce ECL Western Blotting Substrate (Thermo Scientific).

### **V-16. Quantitative reverse transcription-polymerase chain reaction (RT-PCR)**

Total RNA was extracted from cells by TRIzol® Reagent (Invitrogen, Life Technologies, and USA)/chloroform (Wako Pure Chemical Industries, Ltd., Japan) isolation performed using standard methods. Single-stranded cDNA was generated with the

PrimeScript RT-PCR Kit (TaKaRa Inc., Japan) and RT-PCR performed with SYBR Green PCR Master Mix (TaKaRa), both according to the manufacturer's instructions. The primers used are listed in Table 2, including those for *PAX6* (Paired box 6), *NESTIN*, *MUSASHI1*, *GFAP* (glial fibrillary acidic protein), *TUBB3* ( $\beta$ III tubulin), *MAP2* as neural markers and *NANOG*, *KLF4* (Kruppel-like factor 4), *OCT4*, and *BM11* (B cell-specific Moloney murine leukemia virus integration site 1) as markers of stemness, and *BDNF* (brain-derived neurotrophic factor) and *HGF* (hepatocyte growth factor) as neurotrophic factors with *GAPDH* (glyceraldehyde 3-phosphate dehydrogenase) an internal control. The expression of these markers was then normalized to that of *GAPDH*. PCR amplifications were performed in triplicate for each sample.

**Table2. Human primer sequences used for RT-PCR**

Gene		Primer sequence	Product size (bp)
BDNF	Forward	5' AGAGGCTTGACATCATTGGCTG 3'	147
	Reverse	5' CAAAGGCACTTGACTACTGAGC 3'	
BMI1	Forward	5' CGCTTGGCTCGCATTG 3'	148
	Reverse	5' AGCTCAGTGATCTTGATTCTCGTTG 3'	
$\beta$ III-tubulin	Forward	5' CTCAGGGGCCTTTGGACATC 3'	160
	Reverse	5' CAGGCAGTCGCAGTTTTTCAC 3'	
GAPDH	Forward	5' AGCCTCAAGATCATCAGCAATG 3'	111
	Reverse	5' ATGGACTGTGGTCATGAGTCCTT 3'	
GFAP	Forward	5' GGCCCGCCACTTGCA 3'	115
	Reverse	5' GGGAATGGTGATCCGGTTCT 3'	
HGF	Forward	5' TAGGCACTGACTCCGAACA 3'	136
	Reverse	5' AGGAGATGCAGGAGGACAT 3'	
KLF4	Forward	5' ACCTACACAAAGAGTTCCCATC 3'	136
	Reverse	5' TGTGTTTACGGTAGTGCCTG 3'	
Musashi1	Forward	5' CTCCAAAACAATTGACCCTAAGGT 3'	93
	Reverse	5' GACAGCCCCCCCCACAAAG 3'	
MAP2	Forward	5' GGGCCTTTCTTTGAAATCTAGTTT 3'	91
	Reverse	5' CAAATGTGGCTCTCTGAAGAACA 3'	
Nanog	Forward	5' TGGACACTGGCTGAATCCTTC 3'	142
	Reverse	5' CGTTGATTAGGCTCCAACCAT 3'	
Nestin	Forward	5' AACAGCGACGGAGGTCTCTA 3'	220
	Reverse	5' TTCTCTTGTCCCCGCAGACTT 3'	
Oct-4	Forward	5' GACAGGGGGAGGGGAGGAGCTAGG 3'	144
	Reverse	5' CTTCCCTCCAACCAGTTGCCCAAAC 3'	
PAX6	Forward	5' GCTTCACCATGGCAAATAACC 3'	76
	Reverse	5' GGCAGCATGCAGGAGTATGA 3'	

### **V-17. Migration Assays**

The migratory ability of UC-MSCs toward glucose-depleted damaged neural cells was evaluated using a 24-well Transwell chamber (Corning, USA) equipped with an 8- $\mu$ m filter membrane as previously described [44, 45]. Briefly, SH-SY5Y human neuroblastoma cells (DS Pharma Biomedical Co., Ltd., Japan) were cultured in the bottom chamber in DMEM/F12 medium (Wako Pure Chemical Industries, Ltd., Japan) with or without glucose (Wako Pure Chemical Industries, Ltd., Japan). The next day, in the upper chamber, UC-MSCs were plated at  $5 \times 10^4$  cells/well in DMEM/F12 medium containing 10% FBS and co-cultured overnight at 37 °C with 5% CO<sub>2</sub>. Then, non-migratory cells were carefully removed with a cotton swab and the filter membrane was fixed with 4% paraformaldehyde for 20 min and stained with Giemsa (Sigma-Aldrich, Japan). The numbers of trapped cells migrating toward the lower chamber were counted in three random fields under a light scope ( $\times 200$ ).

### **V-18. TUNEL Assay**

To evaluate whether UC-MSC treatment attenuated periventricular cell death, the number of terminal deoxynucleotidyl transferase-mediated dUTP nick-end labeling (TUNEL)-positive cells in the periventricular area were calculated in brain tissue. Briefly, paraffin sections were deparaffinized, rehydrated, and incubated in a solution of 3% H<sub>2</sub>O<sub>2</sub> for 5 min to inhibit endogenous peroxidase activity. Sections were then subjected to the TUNEL

assay using a commercial kit (In Situ Apoptosis Detection Kit, TaKaRa). Apoptotic cells were visualized by DAB staining, and alive cells were counterstained with 3% methyl green. Apoptotic cells were counted in five randomly selected fields at a magnification of 400X using a microscope, and the number of apoptotic cells/total number of cells  $\times$  100% was calculated.

#### **V-19. Fluorescent-labeled inhibitor of caspases (FLICA) labeling**

To evaluate caspase activity in cortical neurons after OGD, Fluorescent-labeled inhibitor of caspases (FLICA) was used (Immunochemistry Technologies, FAM-FLICA® Poly Caspase Assay Kit). The cells were incubated at 37 °C for 1 h with FLICA labeling solution. After washing three times, cells were labeled with propidium iodide (PI), and the images were captured immediately with a fluorescence microscope. PI labeling was used with FLICA to identify four populations of cells: living (FLICA-, PI-); early apoptotic (FLICA+, PI-); late apoptotic (FLICA+, PI+); and necrotic (FLICA-, PI+).

#### **V-20. Cortical neurons proliferation assay**

To evaluate whether co-culture with UC-MSc attenuated cortical neurons death after OGD, cell proliferation was determined using the Cell Proliferation ELISA kit, BrdU (Roche, 11669915001) according manufacturer's instructions. Briefly, BrdU incorporation into

neurons was quantitatively measured by the OD450 measured in a microplate reader (Bio-Rad iMark Microplate Absorbance Reader Version 1.02.01).

#### **V-21. Multiplex flow cytometry beads assay**

Mouse serum and cerebrospinal fluid (CSF) were collected and the concentration of trophic factors secreted from administered UC-MSCs was measured 24 h and 3 weeks after administration using the multiplex beads immunoassay. I evaluated human BDNF, NGF (nerve growth factor), and HGF with the HQ-Plex Kit (Bay Bioscience, Japan). For HGF and BDNF inhibition, HGF and BDNF were depleted from conditioned medium of UC-MSCs using neutralizing antibodies; anti-HGF neutralizing antibody (ab10678, Abcam) and recombinant Human TrkB Fc chimera protein (#688-TK; R&D Systems) as previously reported [36, 46, 47]. Briefly, cells were treated with 0.5 $\mu$ g/mL of anti-HGF antibody or 1 $\mu$ g/mL recombinant Human TrkB Fc chimera protein at plating, and media was not changed during the course of the experiment (48 hours). As a negative control, appropriate recombinant human IgG1 Fc (R&D Systems) was used. For the measurement of the neutralized concentration of HGF and BDNF, the supernatant was analyzed with multiplex flow cytometry beads assay. All samples were analyzed in triplicate according to manufacturers' instructions. Bead fluorescence readings were done by a flow cytometry apparatus (BD™ FACS Canto II). Data were analyzed using FCAP Array ver.3.0.1 Software

(BD Biosciences).

## **V-22. Genomic DNA PCR of human Alu element**

Genomic DNA of mice were extracted from brain, lungs, liver, and spleen using a DNeasy Blood and Tissue Kit (Qiagen) according to the manufacturer's instructions and quantified using a spectrophotometer (NanoDrop 2000; Thermo Fisher Scientific). The human Alu gene, the most abundant repetitive element in the human genome but not present in mice, was amplified by PCR using specific primer pairs for the Alu element [48]. Genomic DNA was extracted from three mice in IVH + UC-MSCs (RM) group as target samples and from the IVH group and normal control group as negative controls. Real-time quantitative PCR (qPCR) was performed with PikoReal™ Real-Time PCR System (Thermo Fisher Scientific). Each reaction consisted of 6.25 µL SYBR Green PCR Master Mix (TaKaRa) supplemented with 1 µL of each primer (10 µmol/L), 3 µL template DNA, and water to a final volume of 12.5 µL. The Alu primer sequences used were as follows: 5-GAGATCGAGACCACGGTGAAA -3 (forward) and 5-TCTCCGCTCACTGCAAGCT -3 (reverse). PCR conditions were as follows: 95 °C for 10 min, 40 cycles (95 °C for 10 s, 60 °C for 50 s, and 72 °C for 1 s), and 40 °C for 30 s. PCR amplifications were performed in triplicate for each sample.

### **V-23. Statistical analysis**

Values are expressed as mean  $\pm$  standard deviation (SD) from three different experiments. Differences between groups were analyzed with JMP 10.0.2 software (SAS Institute, USA). In order to ascertain whether the distributions have normality and equal variances, I performed Shapiro-Wilk tests and F-tests. I then compared the three or four groups using one-way analyses of variance (ANOVAs), followed by Tukey's tests. P-values of 0.05 or less were regarded as statistically significant.

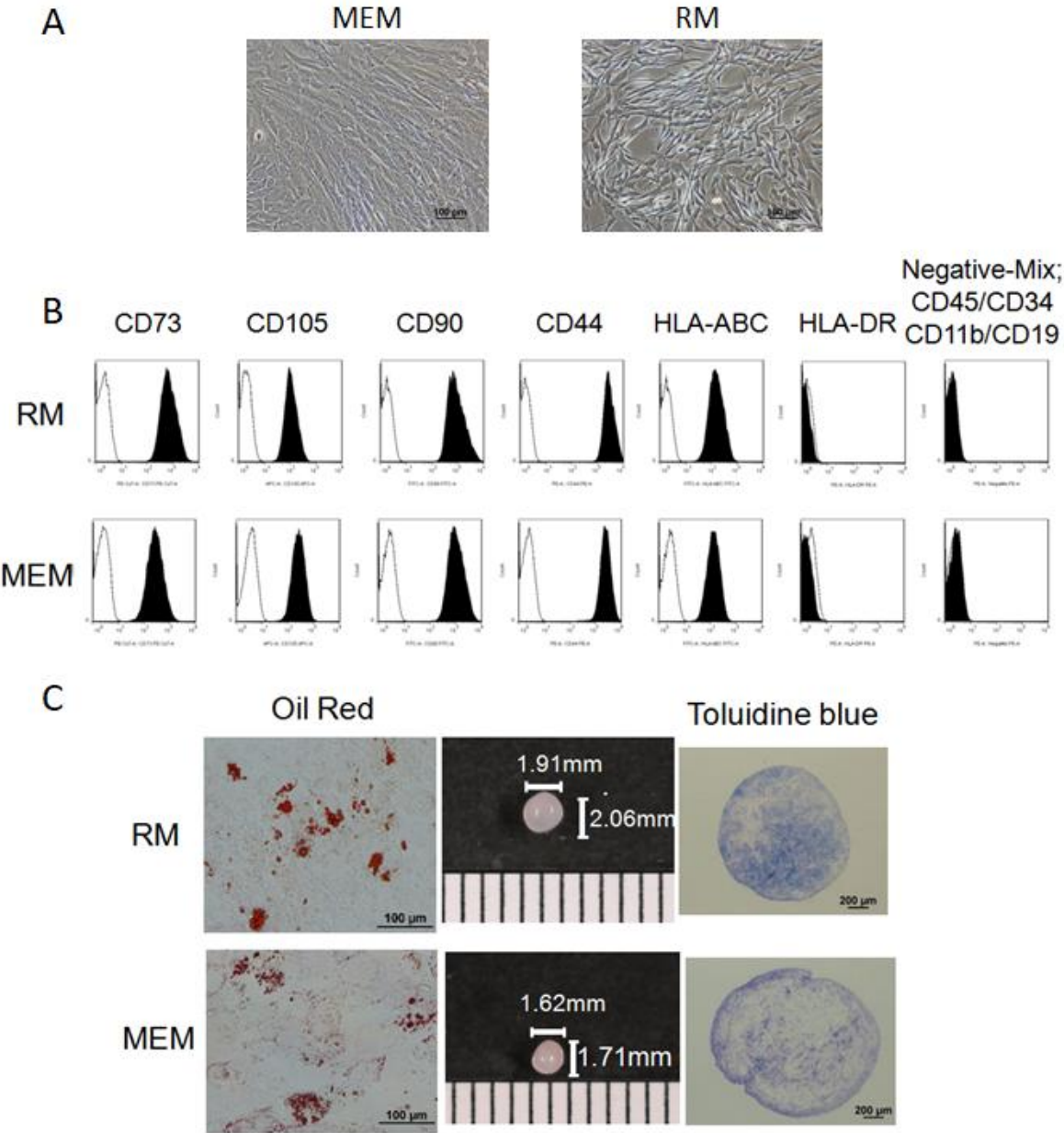
## **VI. Results**

First, in order to apply the serum-free medium RM for clinical use, instead of  $\alpha$ -MEM medium supplemented with 10% FBS, I compared principal characteristics of UC-MSCs cultured with  $\alpha$ -MEM medium containing FBS and RM medium.

### **VI-1. Definitive markers were similar in UC-MSCs cultured with RM or MEM**

UC-MSCs cultured in RM were spindle-shaped plastic-adherent cells, positive for CD73, CD105, CD90, HLA-ABC, and CD44, and negative for CD45, CD34, CD11b, CD 19 and HLA-DR, comparable to those in MEM (Figure 5A-B). UC-MSCs cultured with either RM or MEM could differentiate into adipocytes and chondrocytes (Figure 5C). In adipocyte differentiation medium, red lipid droplets stained by Oil Red O were observed in UC-MSCs cultured with RM or MEM. In chondrogenic differentiation, the elastic firm pellets with diameters of approximately 1.5 mm were observed by the pellet culture system, and toluidine blue staining revealed the presence of extracellular matrix formation in histological sections.

**Figure 5. Characterization and differentiation into adipocyte and chondrocytes of UC-MSCs cultured with  $\alpha$ MEM and RM**



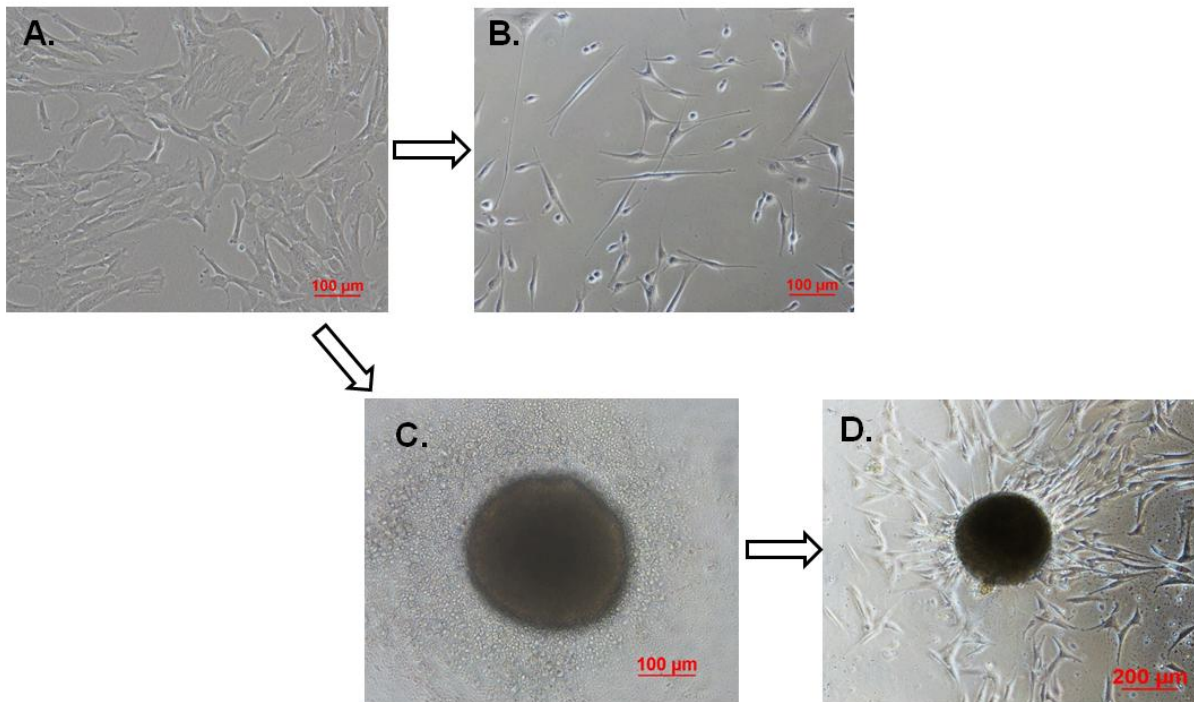
(A) UC-MSCs cultured in RM were spindle-shaped plastic-adherent cells, positive for CD73, CD105, CD90, HLA-ABC, and CD44, and negative for CD45, CD34, CD11b, CD 19 and HLA-DR, comparable to those in MEM. Histogram shows antibody staining (in black) relative to isotype-matched control (white). (B) UC-MSCs cultured with either RM and MEM were differentiated into adipocytes in which the accumulation of Oil Red O-stained lipid drops were observed (Scale bar = 100  $\mu$ m), and chondrocytes in which toluidine blue staining revealed the presence of extracellular matrix with metachromasia in histological sections (Scale bar = 1mm, 200  $\mu$ m respectively).

## VI-2. Neurosphere formation and neurogenic differentiation of UC-MSCs

UC-MSCs plated in the adherent culture dishes showed spindle shaped, a fibroblast-like morphology (Figure 6A), with elevated proliferation levels. However, cells shifted to a neuronal-like bipolar morphology, with long thin processes and a depressed proliferation rate, in response to culturing in neurogenic differentiation medium for about 72 to 78 h (Figure 6B). Alternatively, when UC-MSCs were suspended in medium supplemented with EGF and bFGF and plated in low attachment 96-well plates, the cells began to aggregate and form clusters defined as neurospheres (UC-MSC-neurospheres) within 3–7 days (Figure 6C). The diameter of spheres were  $380.3 \pm 37.8 \mu\text{m}$  ( $n = 8$ ) and consisted of  $1.0 \pm 0.23 \times 10^4$  cells with more than 90% viable cells as determined by counting with trypan blue staining after dissociation ( $n = 8$ ).

For further neurogenic differentiation experiments, the UC-MSC-neurospheres were isolated and re-plated in 24-well tissue culture plates with neurogenic differentiation medium. Spheroids gradually started to expand in all directions while maintaining a spherical shape at the center, whereas differentiated cells from UC-MSC-neurospheres exhibited classical neuronal-like bipolar morphology with formation of long thin processes (Figure 6D). I also characterized the migrating cells from differentiated UC-MSC-neurospheres; the cells still exhibited the surface markers of MSCs criteria (data not shown).

**Figure6. Neurogenic differentiation and neurosphere formation of UC-MSCs**



(A) UC-MSCs plated in the adherent culture dish showed spindle shaped, a fibroblast-like morphology, and (B) were induced to neural phenotype changing their morphology toward neuronal-like bipolar morphology, with formation of long thin processes with neurogenic differentiation medium. (C) UC-MSCs suspended in the medium in supplemented with EGF and bFGF and plated in low attachment plates in suspension began to aggregate to form neurospheres within 3–7 days. (D) UC-MSC-neurospheres re-plated in tissue culture plates with neurogenic differentiation medium started to expand toward all directions keeping its sphere shape at the center and exhibited neuronal-like bipolar morphology with formation of long thin processes (Scale bar = 100 μm). The data shown are representative of three independent experiments.

### **VI-3. Neural marker expression in UC-MSC- and UC-MSC-neurosphere-derived cells**

The expression of neural biomarkers was compared amongst cells derived from four groups: (1) undifferentiated UC-MSCs, (2) differentiated UC-MSCs, (3) undifferentiated UC-MSC-neurospheres, and (4) differentiated UC-MSC-neurospheres.

As determined by immunohistochemistry, there were more MAP-2-, MUSASHI-1-, GFAP-, and Nestin-positive cells in differentiated UC-MSCs and differentiated UC-MSC-neurospheres compared to their undifferentiated counterparts. PAX6 was faintly positive only in differentiated UC-MSC-neurospheres, whereas  $\beta$ III-tubulin expression was observed regardless of differentiation and neurosphere formation (Figure 7). I also examined their protein expression by immunoblotting experiments; their expression was not inconsistent with the results of immunocytochemistry (Figure 8). In order to quantify the neurogenic differentiated cells, I counted the proportion of positive cells in both, MAP-2 and Musashi1 in four groups, and the results showed that the differentiated UC-MSC-neurosphere group displayed the highest proportion of positive cells in both, MAP-2 and Musashi1 staining (data not shown). Differentiated UC-MSCs and differentiated UC-MSC-neurospheres showed a higher proportion of MAP-2- and Musashi-1-positive cells compared with their undifferentiated counterparts.

**Figure7. Immunocytochemistry of neural markers expression of UC-MSCs and neurospheres before and after neural differentiation**

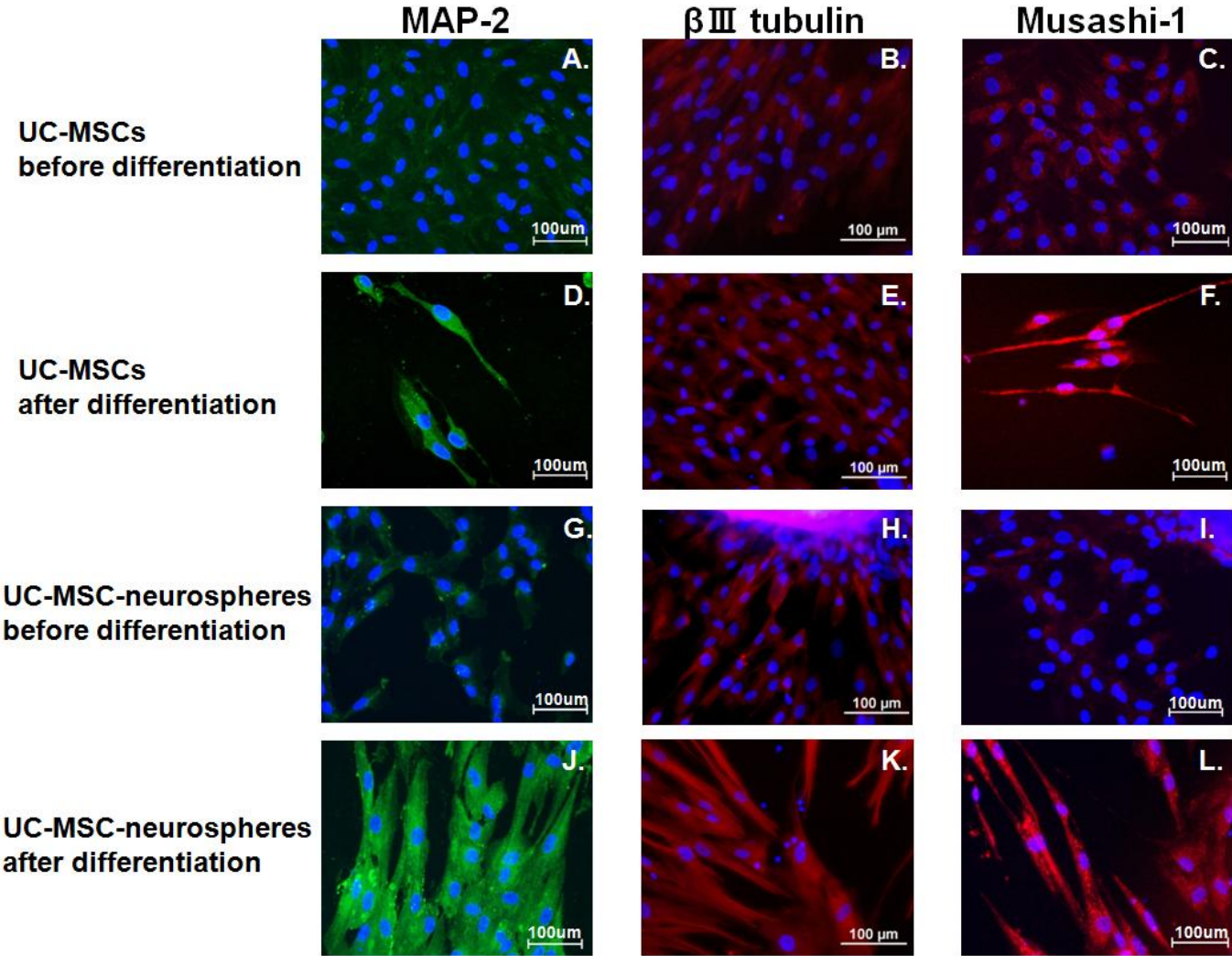
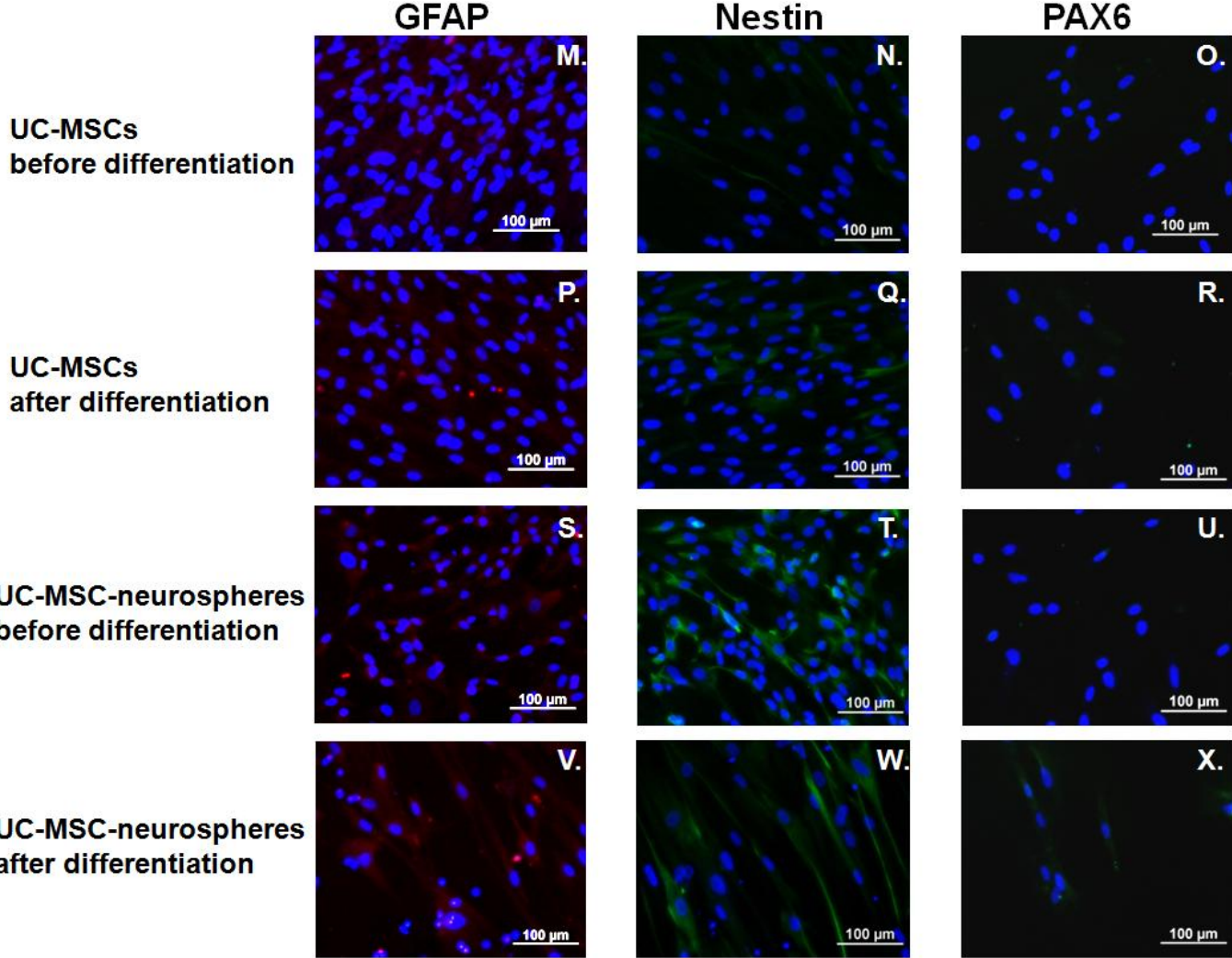
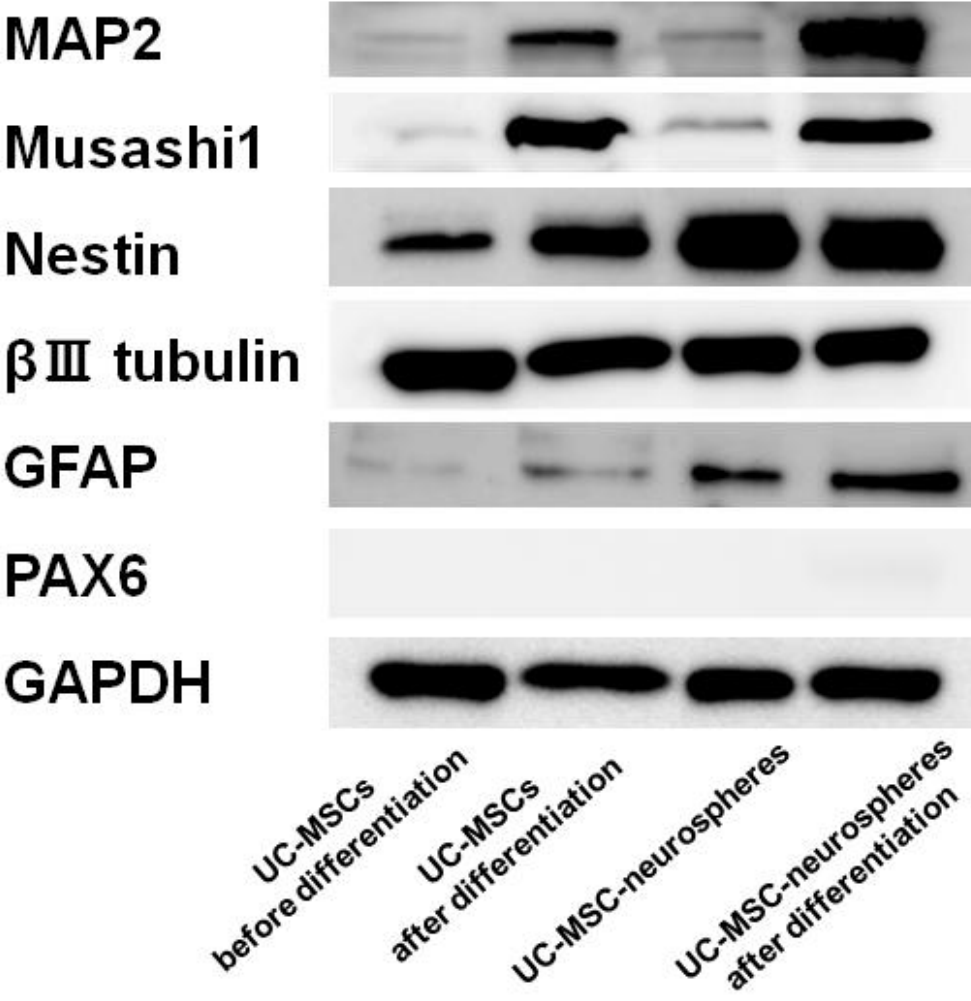


**Figure7 (continued). Immunocytochemistry of neural markers expression of UC-MSCs and neurospheres before and after neural differentiation**



Immunocytochemistry of UC-MSCs before differentiation (A-C, M-O), UC-MSCs after differentiation (D-F, P-R), the cells migrating from neurospheres (G-I, S-U), and the cells migrating from neurospheres after differentiation (J-L, V-X) are shown. (Scale bar = 100 μm).

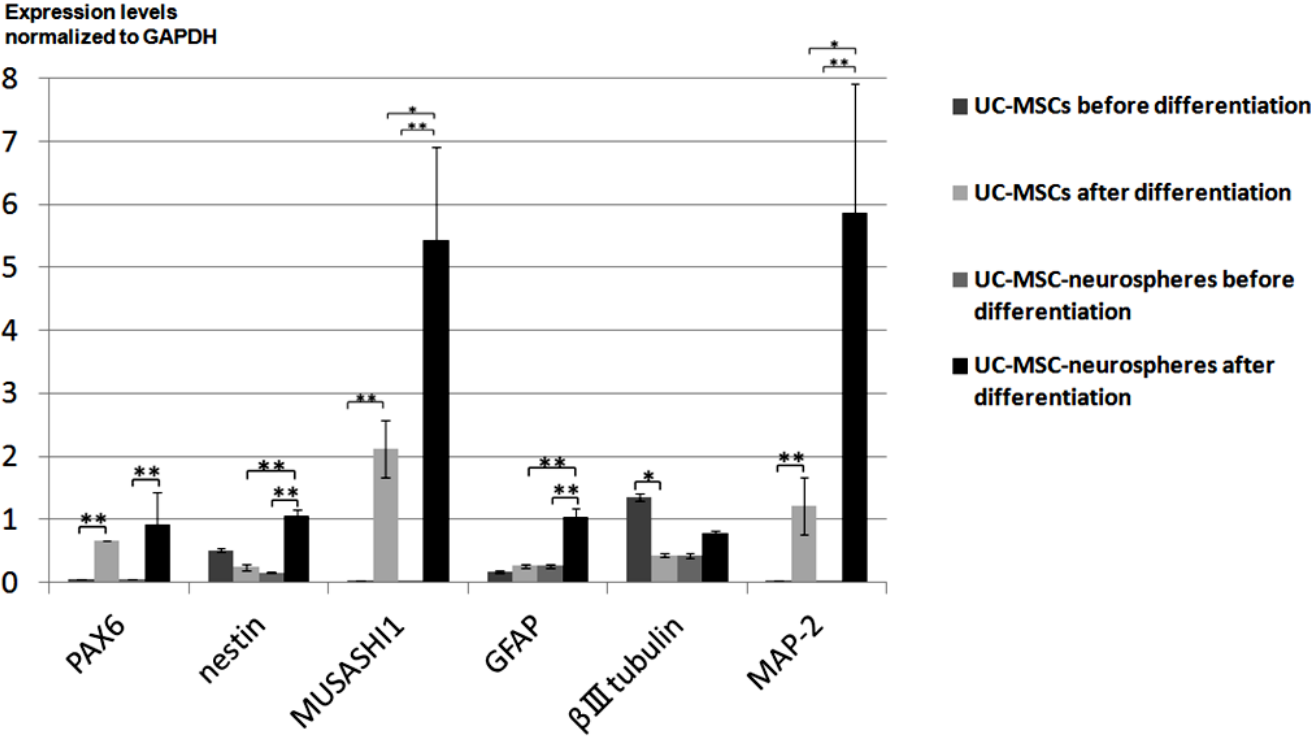
**Figure8. Western blotting of neural marker expression of UC-MSCs and neurospheres before and after neural differentiation**



Expression of neural markers was analyzed by western blotting. GAPDH was used as an internal control. The data shown are representative of three independent experiments.

In gene expression analysis by qRT-PCR, *PAX6*, *MUSASHI1*, and *MAP2* exhibited significantly higher expression in differentiated cells than their undifferentiated counterparts. However, GFAP and NESTIN were induced in differentiated UC-MSCs-neurospheres, but not in UC-MSCs cultured in the presence of differentiation medium. As with the results of immunocytochemistry and immunoblotting,  $\beta$ III tubulin was expressed in undifferentiated UC-MSCs and was not affected by the presence of neurogenic differentiation medium. The cells from differentiated UC-MSCs-neurospheres expressed the neural progenitor markers *PAX6*, NESTIN, and *MUSASHI1*; the mature neuron marker *MAP2*; and the mature astrocyte marker GFAP at significantly higher levels than differentiated UC-MSCs (Figure 9). We also compared the expression of these neural markers in UC-MSCs and SH-SY5Y cells as a positive control by RT-PCR, and the expression of neural markers in UC-MSCs were much lower than those in SH-SY5Y cells (data not shown).

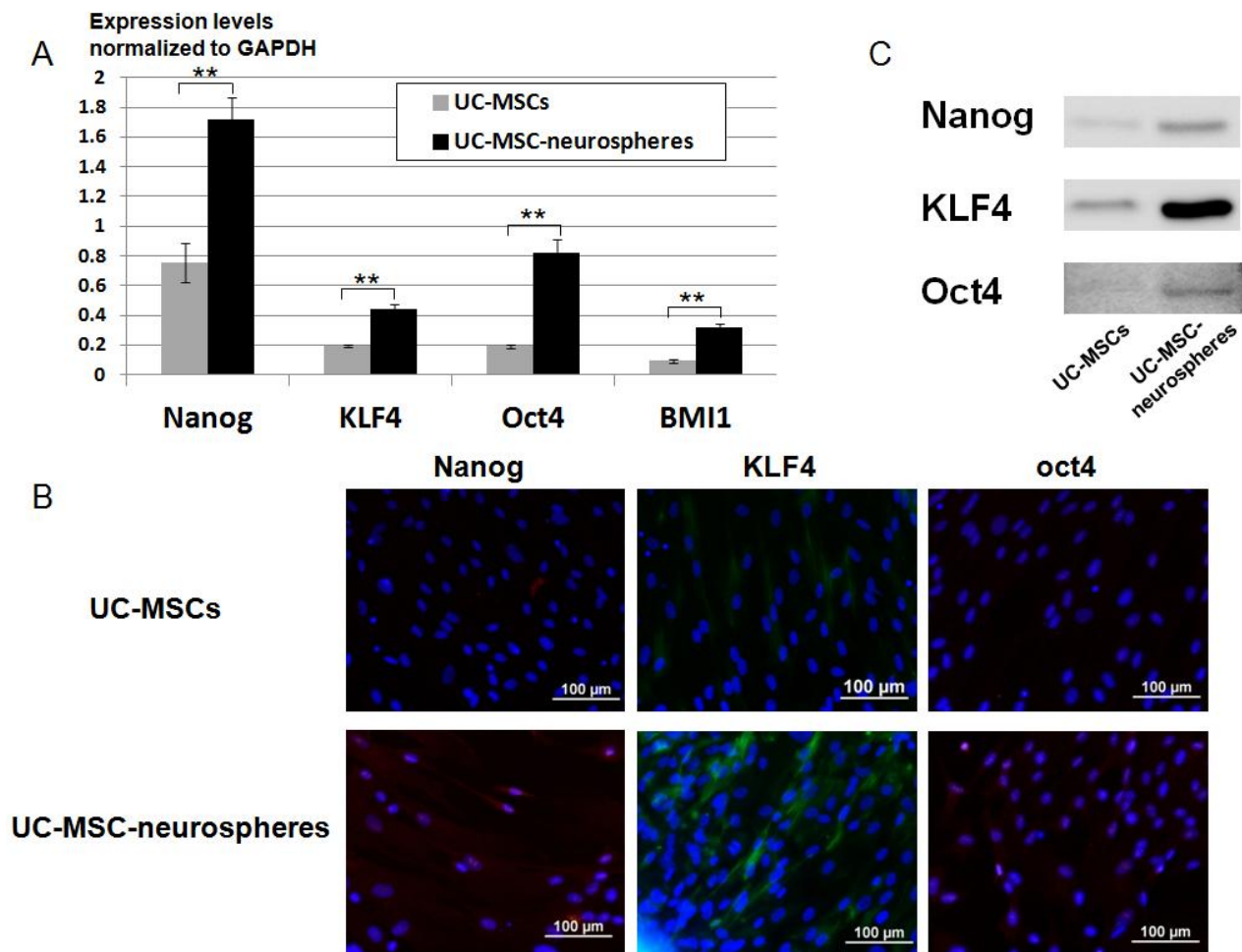
**Figure9. Quantitative analysis of neurogenic differentiation of UC-MSCs and UC-MSC-neurospheres**



The graph shows the quantitative analysis of the neural marker expression of UC-MSCs and UC-MSC-neurospheres before and after neural differentiation by RT-PCR. The expression of neural markers was normalized to that of GAPDH. Triplicate PCR amplifications were performed for each sample, and the results are represented as mean values of three different samples ± SD. \*P < 0.05; \*\*P < 0.01.

Interestingly, in addition to the neural markers, the expression of embryonic stem cell markers, *NANOG*, *OCT4*, *KLF4*, and *BM11* was higher in UC-MSc-neurospheres as compared to UC-MSCs, as shown by results from RT-PCR (Figure 10A). The immunostaining (Figure 10B) and immunoblotting (Figure 10C) for *NANOG*, *OCT4*, and *KLF4* demonstrated equivalent results. We also compared the expression of these stemness markers in UC-MSCs and induced pluripotent stem (iPS) cells derived from UC-MSCs as a positive control by RT-PCR, and the expression of *NANOG* and *OCT4* in UC-MSCs were much lower than those in iPS cells (data not shown).

**Figure10. Expression of stemness markers in UC-MSCs and UC-MSC-neurospheres.**

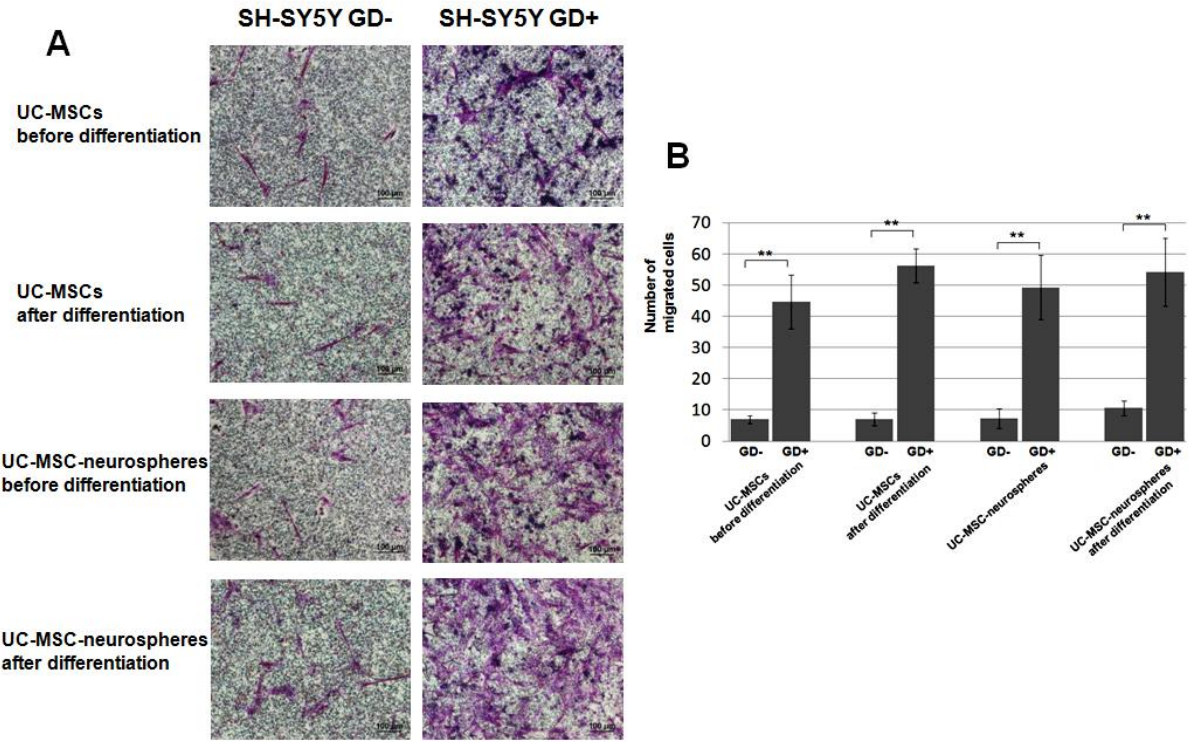


The graph shows the quantitative analysis of stemness markers expression of UC-MSCs and UC-MSC-neurospheres before and after neural differentiation by RT-PCR. The expression of stemness markers was normalized to that of GAPDH, respectively (A). Immunocytochemistry of UC-MSCs and UC-MSC-neurospheres are shown. The expression of Nanog, KLF4, and oct4 was higher in UC-MSC-neurospheres than that in UC-MSCs (B). (Scale bar = 100  $\mu$ m). Western blotting results showed higher expression of Nanog, KLF4, and oct4 in UC-MSC-neurospheres than in UC-MSCs (C). The data shown are representative of three independent experiments.

#### **VI-4. Migration ability of UC-MS- neurospheres**

MSCs are known to migrate toward sites of tissue damage. I examined the migration ability of UC-MS- and UC-MS- neurospheres toward normal or glucose-depleted SH-SY5Y cells using Transwell migration assays. The number of migrating cells co-cultured with glucose-depleted SH-SY5Y cells was significantly higher compared to that with normal SH-SY5Y cells in all groups. (Figure 11A-B). However the number of migrating cells co-cultured with glucose-depleted SH-SY5Y cells was equivalent among four groups.

**Figure11. Migration of UC-MSC-neurospheres toward glucose-depleted cells**

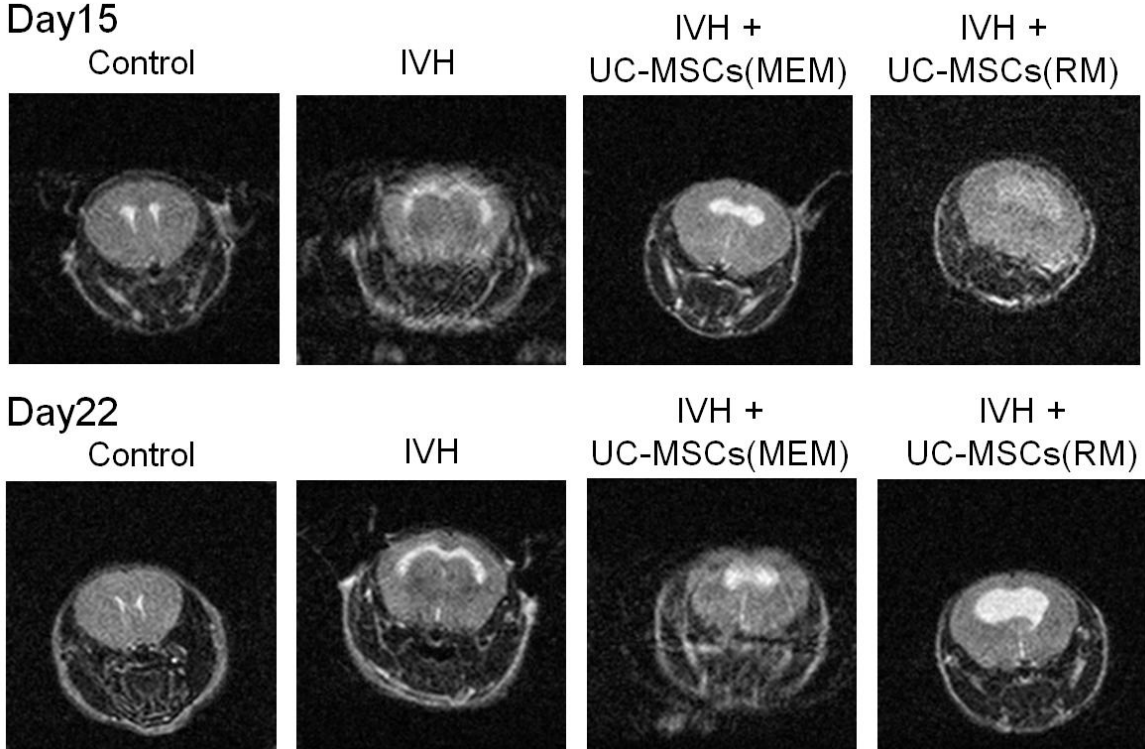


Transwell filter membranes were fixed and stained with Giemsa (Scale bar = 100 μm). In all groups, the number of migrating cells co-cultured with glucose depleted cells increased compared with those with non-depleted cells. (GD; Glucose depletion). The quantitative analysis of cell migration is shown, and results are represented as mean values of three four different samples ± SD (CI). \*\*P < 0.01.

## **VI-5. IVH surgery induced ventricular dilatation evaluated by MRI**

Next, in order to investigate whether the UC-MSCs can rescue the neonatal encephalopathy *in vivo*, I first established neonatal intraventricular hemorrhage (IVH) mice model, one of neonatal encephalopathy, followed by the intravenous injection of UC-MSCs. The neonatal IVH mouse model was made by the injection of blood into the right ventricle and those mice indicated ventricular dilatation confirmed by brain MRI. T2-weighted brain MRI in the IVH group showed ventricular dilatations filled with hemorrhagic fluid at 10 and 17 days after IVH (at P15 and P22, respectively; Figure 12). UC-MSC administration failed to diminish the ventricular dilatation in size at P15 in IVH + UC-MSCs (MEM) and IVH + UC-MSCs (RM) groups. Similarly, the size of ventricular dilatation was not different between UC-MSC administration groups at P22.

**Figure12. T2-weighted MRI in IVH neonatal mice with or without UC-MSCs**



T2-weighted brain MRI in the IVH group showed ventricular dilatations filled with hemorrhagic fluid (white lesion) at 10 and 17 days after IVH (at P15 and P22, respectively). The data represent five individual experiments.

## **VI-6. UC-MSc administration improved behavioral outcome**

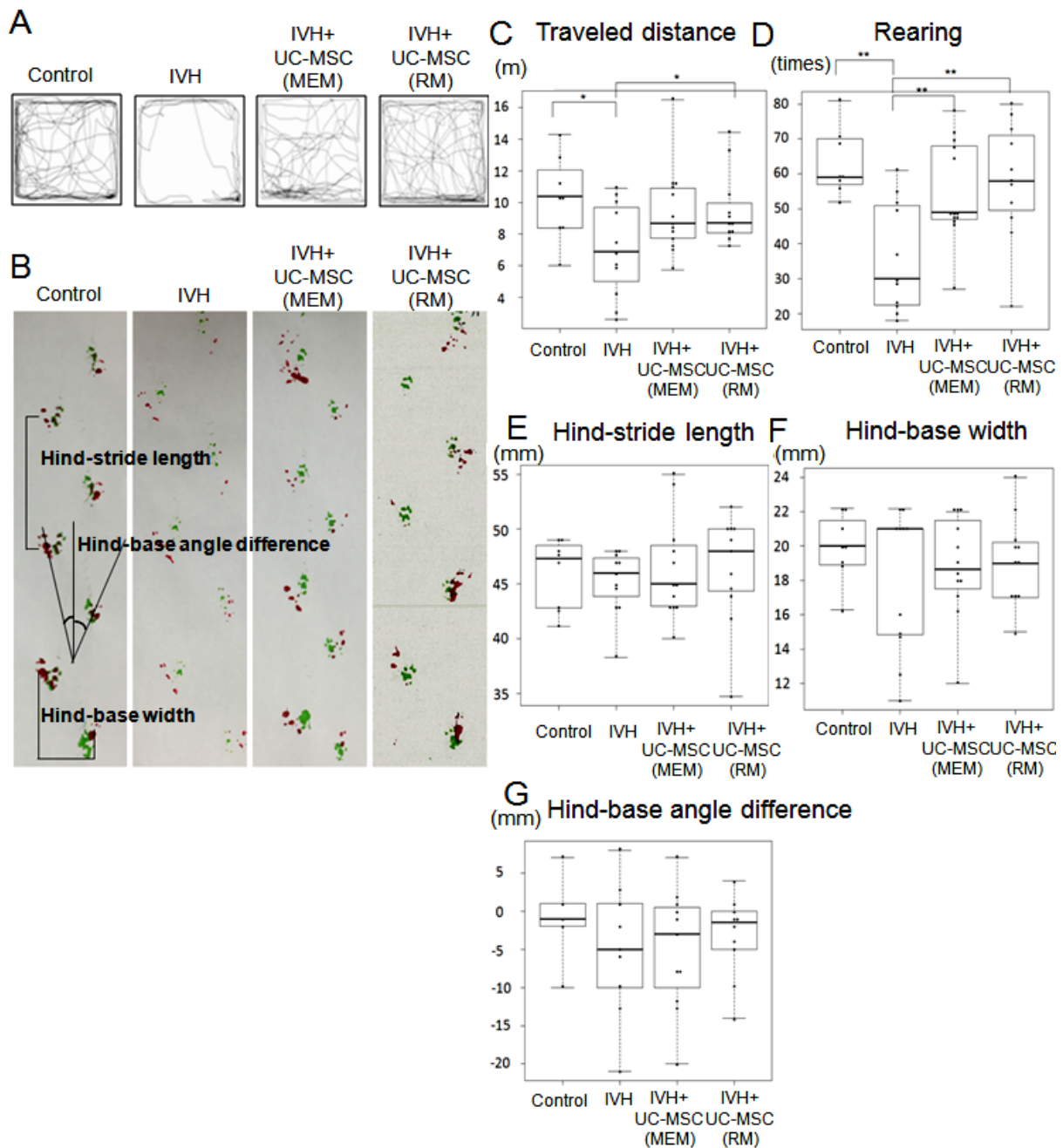
Next, I examined the effect of UC-MSc administration on neurological behavior in the neonatal mice after IVH. Although the ventricular dilatation evaluated by MRI was not changed within the study period, UC-MSc administration significantly improved the behavioral functions measured by the open field test. The mice in the IVH group stayed close to the wall resulting in poor traveling compared to those in the Control group, which explored the whole area as they habituated to the new environment and anxiety decreased (Figure 13A). UC-MScs cultured with RM or MEM improved traveling distance. Quantitative analysis of travel distance revealed that the mice in the IVH group traveled a significantly shorter distance compared to those in the Control group, whereas the mice in the IVH + UC-MScs (MEM) and (RM) groups demonstrated increased travel distance. Notably, the mice in the IVH + UC-MScs (RM) group exhibited a significant difference in travel distance compared with those in the IVH group ( $p=0.0494$ ), while the IVH + UC-MScs (MEM) group showed a non-significant improvement (Figure 13C). I also evaluated how the rearing number was affected by IVH. The mice in the IVH group showed significantly decreased rearing number compared to those in the Control group. UC-MScs significantly improved the impairment of rearing in both IVH+UC-MScs (RM) and (MEM) ( $p=0.0010$ ; Figure 13D).

I next performed footprint analysis; hind-stride length, hind-base width (the distance between right and left hind-limb strides), and hind-base angle difference (the difference in

angle from the median line between right and left hind-base) were calculated and compared among the four groups (Figure 13B). In quantitative analysis, although there were no significant differences among the four groups in hind-stride length and hind-base width (Figure 13E-F), there was a tendency of abduction to the left side in the IVH group compared to in the Control group (Figure 13G).

These results demonstrate equivalent outcomes for UC-MSCs cultured with RM and those with MEM in the IVH treatment model. Therefore, the following experiments were performed using only UC-MSCs cultured with RM, indicated as the IVH + UC-MSCs group.

**Figure13. Neurological behavioral assessment**



(A) Open field test was performed at P23, and overall activity in the box was recorded with video-monitor. (B) Representative sample of foot-print analysis; (i) hind-stride length, (ii) hind-base width (the distance between the right and left hind-limb strides), and (iii) hind-base angle difference (the difference in angle from the median line between right and left hind-base) were calculated and compared between four groups. Quantitative analysis of (C) traveled distance and (D) rearing in open-field test. (E-G) Quantitative analysis of foot-print test. Three trials were performed in each experiment. \* $p < 0.05$  and \*\* $p < 0.01$ . (Control;  $n=8$ , IVH;  $n=11$ , IVH + UC-MSCs (MEM);  $n=13$ , IVH + UC-MSCs (RM);  $n=11$ )

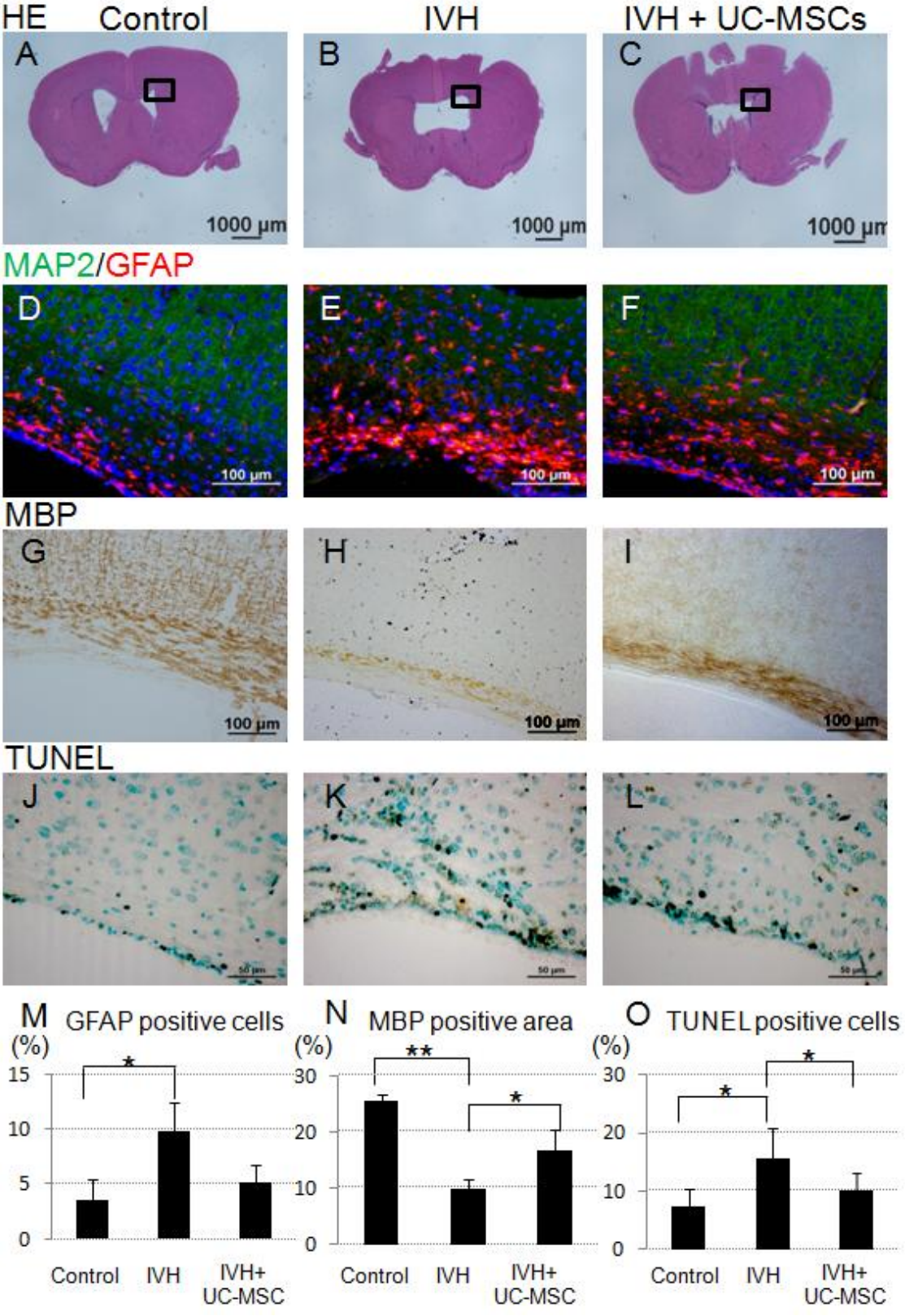
## **VI-7. UC-MSC administration attenuated reactive gliosis resulting in the maintenance of white matter thickness in IVH mice**

I investigated the effect of UC-MSC administration on reactive gliosis in the IVH model [43, 49-51]. Using immunohistochemistry, I found that the IVH group exhibited more GFAP-positive glial cells in the periventricular area than Control group. I also found that reactive gliosis was attenuated in the IVH + UC-MSCs group (Figures 14D-F and 14M), although no significant difference was observed between the IVH and IVH + UC-MSCs groups.

Contrary to the increase of the GFAP-positive glial cells in the periventricular region in the IVH group, MBP-positive myelin cells, which form white matter, were decreased resulting in a decrease of white matter thickness, defined as hypomyelination (Figure 14G and H). UC-MSC administration attenuated the thinning of white matter (Figure 14I). While white matter thickness was significantly decreased in the IVH group, this reduction was significantly attenuated in the IVH + UC-MSC group ( $p=0.0039$ ; Figure 14N).

Evaluating apoptotic cells using TUNEL staining in the periventricular area damaged by IVH, I found that apoptosis was rescued by UC-MSC administration. TUNEL-positive apoptotic cells in the periventricular area were more numerous in the IVH group than in the Control group, and they were reduced in the IVH + UC-MSCs group compared to the IVH group ( $p=0.028$ ; Figure 14J-L, O).

**Figure14. Immunohistochemistry of neonatal mouse brain with or without UC-MSCs**



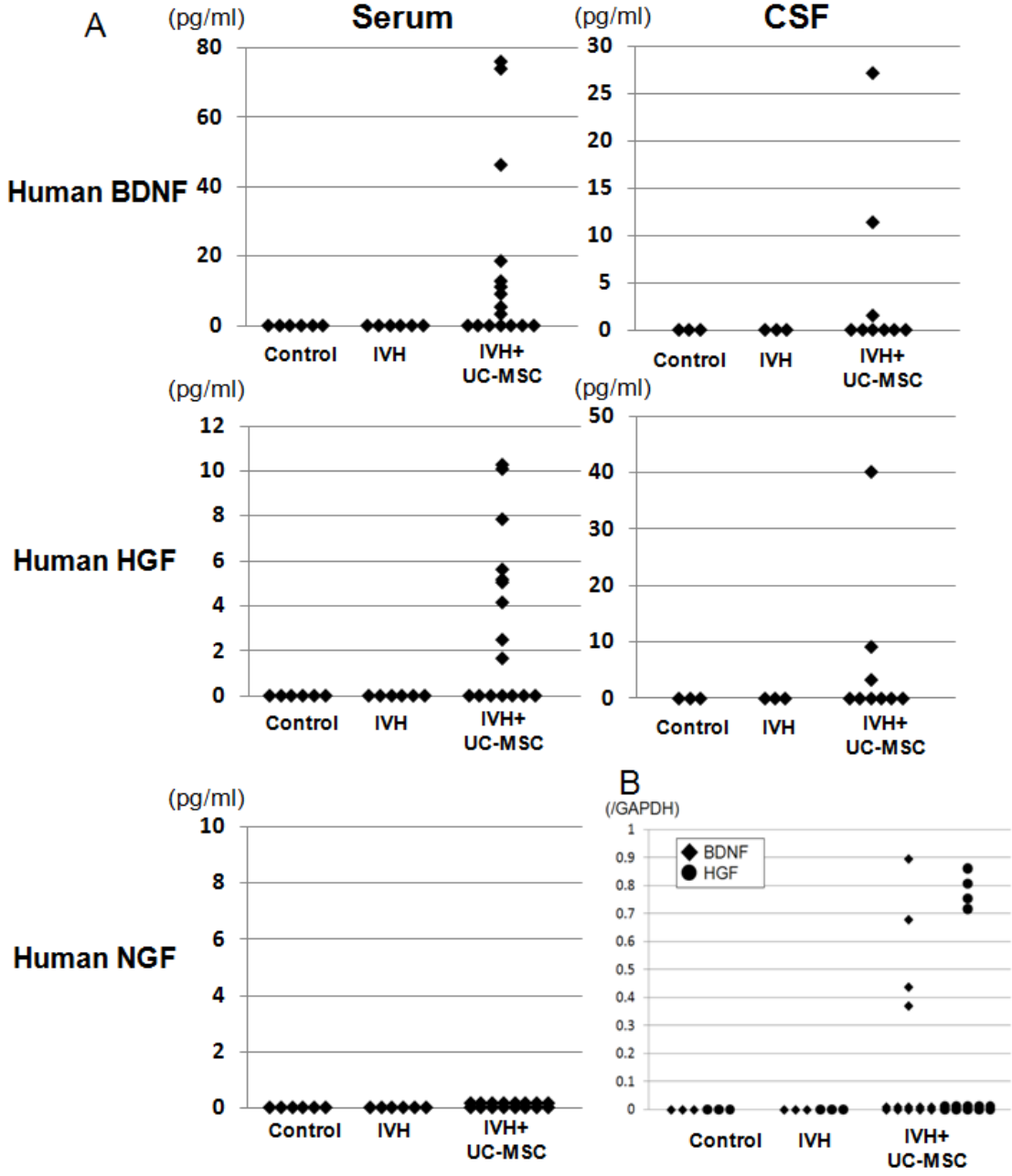
(A-C) Hematoxylin and eosin (HE) staining of neonatal mouse brain (Scale bar = 1000  $\mu$ m). Mouse brain of Control group (left column), IVH group (middle column) and IVH +

UC-MSCs group (right column) are shown. (D-F) MAP2 (green) and GFAP (red) staining. (Scale bar = 100  $\mu\text{m}$ ). (G-I) MBP staining of periventricular myelination. (Scale bar = 100  $\mu\text{m}$ ). (J-L) Apoptosis detection using TUNEL assay. (Scale bar = 50  $\mu\text{m}$ ). (M-O) Quantitative analysis of GFAP positive cells (M), MBP positive area (N), and TUNEL positive cells (O). The quantitative analysis are represented as mean values of three different samples  $\pm$  SD. \* $p < 0.05$  and \*\* $p < 0.01$ .

## **VI-8. Human-BDNF and HGF were detected only in IVH mice with UC-MSC administration**

Based on the above results, UC-MSCs significantly improved functional and histopathological outcomes in IVH mice. To assess the key factors in the repair of damaged tissue in the IVH + UC-MSCs group, mouse sera and CSF were collected, and human BDNF, NGF, and HGF were measured using the multiplex beads immunoassay. Regarding mouse sera, in 9 of 16 mice of the IVH + UC-MSCs group, human BDNF and HGF were elevated 24 h after administration of UC-MSCs, while neither factor was detected in control and IVH groups. NGF, however, was not detected in the IVH + UC-MSCs group (Figure 15 A). And also human BDNF and HGF were elevated in 3 of 9 mice CSF of the IVH + UC-MSCs group 24 h after administration of UC-MSCs. RT-PCR results also revealed these trophic factors were elevated in 4 of 14 mice brain tissue of the IVH + UC-MSCs group 24 h after administration of UC-MSCs (Figure 15 B). Human BDNF, HGF, and NGF were not detected 3 weeks after UC-MSC administration (data not shown).

**Figure15. Human-BDNF, HGF, and NGF measured in mouse sera, cerebrospinal fluid and brain tissues.**



(A) Mouse sera and cerebrospinal fluid (CSF) were collected 24hours and 3weeks after UC-MSCs administration and human BDNF, HGF, and NGF concentration were measured using the multiplex beads immunoassay. Triplicate assays were performed for each sample. (Control; n=6, IVH; n=6, IVH + UC-MSCs; n=16 in sera assay, and Control; n=3, IVH; n=3, IVH + UC-MSCs; n=9 in CSF assay, respectively). (B) Human-BDNF and HGF expression in brain tissue using quantitative RT-PCR (Control; n=3, IVH; n=3, IVH + UC-MSCs; n=9). The expression of markers was normalized to that of GAPDH

## **VI-9. Human UC-MSCs were detected in the brain and lung of IVH mice after intravenous injection**

To trace the UC-MSCs in IVH mice, I transfected the luciferase gene into UC-MSCs and performed *in vivo* imaging analysis. The luminescent signal in mice was traced at indicated time points after intravenous administration of UC-MSCs using the *in vivo* imaging system. In the mice injected with UC-MSCs, prominent luminescent signals were detected first in the lung at 6 h, spreading to the neck and head by 3 days after intravenous injection, and then declining in subsequent days (Figure 17A). No luminescent signals were detected in the IVH + UC-MSCs group 21 days after injection of UC-MSCs. No signals were detected in the mice of the Control and IVH groups at any time point.

Furthermore, I attempted to detect injected UC-MSCs in IVH mice organs using genomic DNA PCR of the human Alu element. The human Alu gene, the most abundant repetitive element in the human genome but not present in mice, was amplified by quantitative PCR. Genomic DNA was extracted from brain, lungs, liver and spleen of RM group mice. At first I investigated quantification of UC-MSCs according to Alu sequence determination *in vitro* (Table 2). High amounts of mouse brain DNA produced nonspecific amplification with an average Ct of  $31.92 \pm 0.21$  cycles. A Small amount of mouse DNA could not be detected (Samples 2 and 3). In samples containing human UC-MSCs DNA (Samples 4 to 6) or a mixture of human and mouse DNA (Samples 7 to 15), a rise in Ct was

associated with a decrease in human DNA content. Next I quantified UC-MSCs according to Alu sequence determination. Figure 16 shows determination of the number of Alu sequences according to the percentage of UC-MSCs in mixed populations of human UC-MSCs and mouse DNA. The relationship between the number of human UC-MSCs and the Alu signal was strong with a correlation coefficient of  $r = -0.9137$ . Alu genes were detected 1 day after UC-MSC injection mostly in lungs and brains. However, Alu elements were not detected 3 weeks after UC-MSC injection (Figure 17B). From the standard curve of Alu quantification, of intravenous injected  $1 \times 10^5$  cells, at most 133 cells were detected in the brain and 287 cells in the lung. Moreover, I examined the localization of the injected UC-MSCs as detected by fluorescent anti-HLA Class 1 and CD105 antibodies in the mouse brain 24 h after UC-MSC injection. HLA Class 1 and CD105 double positive cells were observed in the perivascular region of the mouse brain in the IVH + UC-MSCs group (Figure 17C) but not in the Control and IVH group without UC-MSCs (data not shown).

**Table2. Quantification of UC-MSCs according to Alu sequence determination**

sample	UC-MSCs DNA	Mouse brain DNA	Ct	Ct SD	Tm
sample 1	0	100ng	31.92	0.2121	87.2
sample 2	0	10ng	Negative		
sample 3	0	1ng	Negative		
sample 4	10ng	0	14.05	0.1622	86.8
sample 5	1ng	0	17.32	0.0346	86.6
sample 6	100pg	0	20.5625	0.0623	86.6
sample 7	10ng	100ng	14.06	0.0871	87.2
sample 8	2ng	100ng	16.688	0.1937	87.2
sample 9	1ng	100ng	17.29	0.4045	87.4
sample 10	100pg	100ng	21.704	0.4814	87.2
sample 11	20pg	100ng	22.605	0.1352	87.2
sample 12	10pg	100ng	25.43	0.0848	87.2
sample 13	2pg	100ng	27.05	0.1606	87.2
sample 14	1pg	100ng	29.5533	0.7617	87
sample 15	0.1pg	100ng	31.735	0.3807	87.2

**Figure16. Standard curve of Ct value by %UC-MSCs proportion in mouse brain**

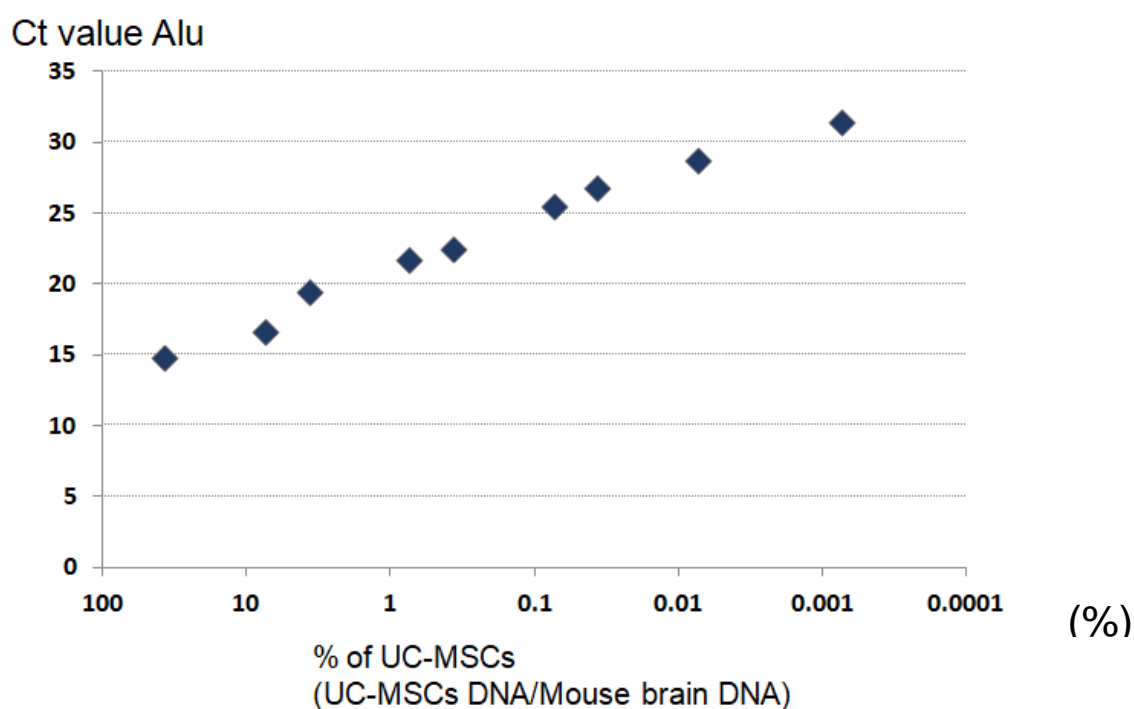
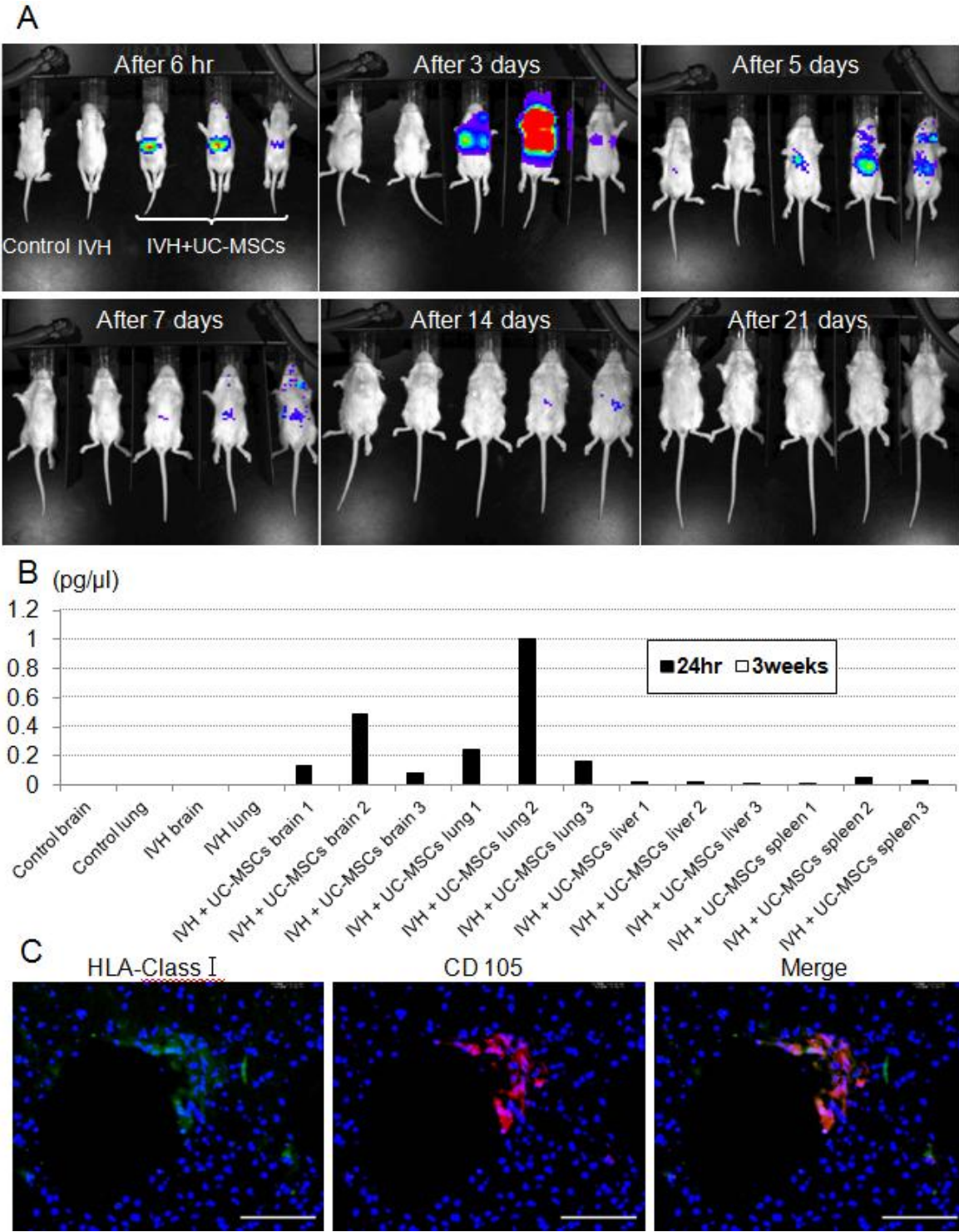


**Figure17. Tracking and detection of UC-MSCs administered intravenously**



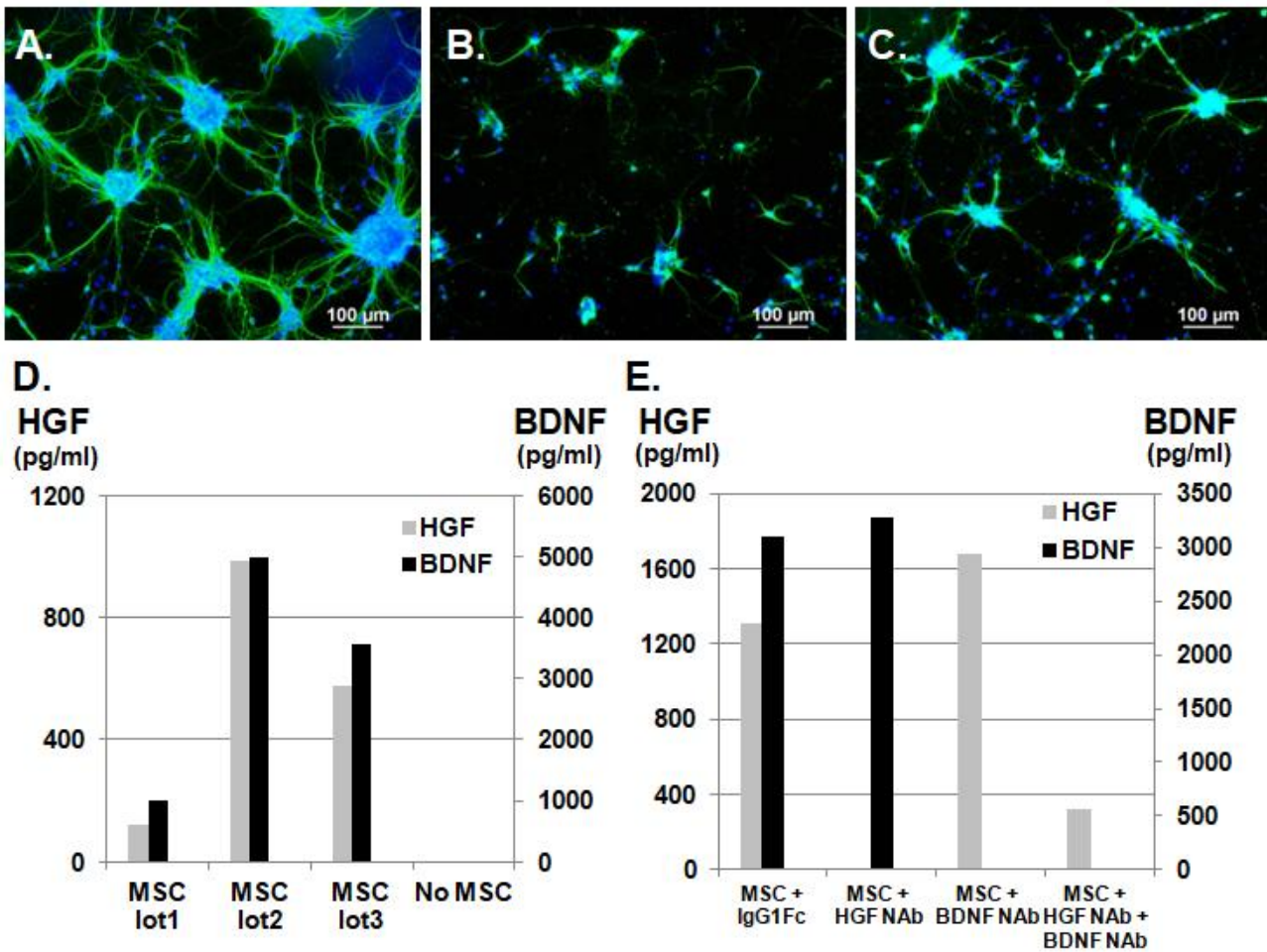
(A) Representative IVIS images are shown. For UC-MSC in vivo imaging, mice were examined at different time points after UC-MSC administration using the IVIS. All pictures were taken at the same threshold of sensitivity. (B) Detection of injected UC-MSCs in organs by genomic DNA PCR of human Alu element. (C) HLA Class 1 (green), CD105 (red), and merge of the mouse brain in the IVH + UC-MSCs group. Double positive cells were observed in the perivascular region (Scale bar = 50 μm).

## **VI-10. Constitutive secretion of HGF and BDNF from UC-MSCs co-cultured with cortical neurons after OGD**

I found that the intravenous injection of UC-MSCs improved behavioral outcome in IVH, by restoring periventricular reactive gliosis, hypomyelination, and periventricular cell death *in vivo*, and that transplanted UC-MSCs migrated towards injured brain, but disappeared three weeks after injection secreting HGF and BDNF. Next I proved the validity of mechanisms *in vitro* using primary mouse neuron injury model. Primary cultures of neonatal cortical neurons exhibited typical morphology, showing a neurite outgrowth-forming network (Figure 18A) that could be visualized by positive MAP-2 labeling in green, which represented mature neurons. Neurites and neuronal clusters disappeared after OGD (Figure 18B), but co-culture with UC-MSCs restored mature neurons, long neurites, and cluster formations (Figure 18C). Using a multiplex flow cytometry bead assay to analyze HGF and BDNF concentrations in medium containing UC-MSCs confirmed that both factors were constitutively secreted from UC-MSCs, and that their concentrations varied by UC-MSC lot (n = 3, Figure 18D). Importantly, HGF and BDNF concentrations could be appropriately reduced by the addition of NAb (Figure 18E). Using these methods, the following experiments were performed: (1) control, (2) neurons injured by OGD (OGD), (3) neurons injured by OGD co-cultured with UC-MSCs (OGD+MSC), (4) OGD + MSC with anti-HGF NAb (OGD+MSC+ HGF NAb), (5) OGD + MSC with anti-BDNF NAb (OGD+MSC+BDNF

NAb), and (6) OGD + MSC with both anti-HGF NAb and anti-BDNF NAb (OGD+MSC+  
HGF NAb + BDNF NAb).

**Figure18. HGF and BDNF secreted from UC-MSCs**

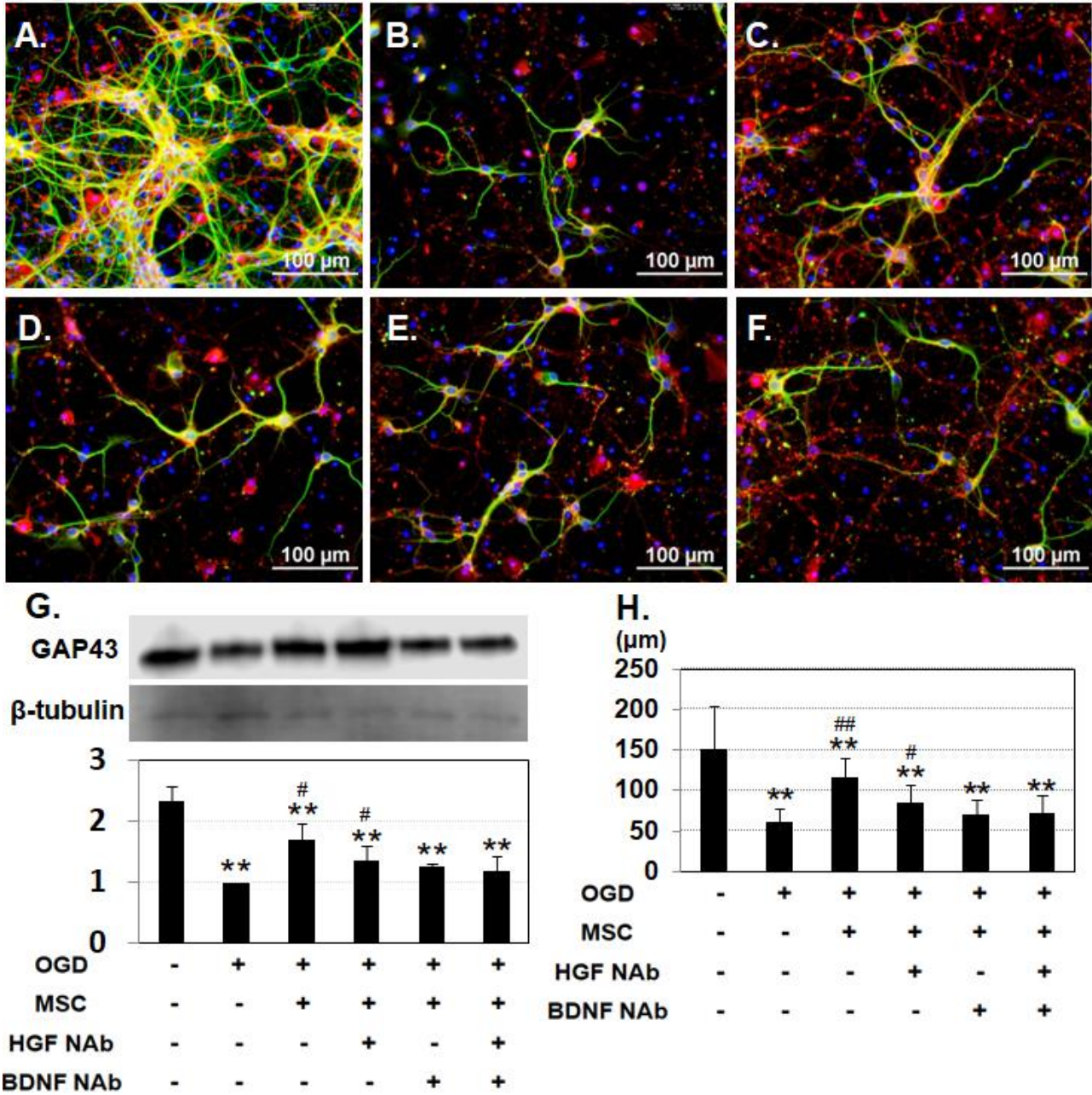


Cortical neurons after OGD co-cultured with UC-MSCs were stained with MAP2. Mature neurons were stained in green, and nuclei were counterstained with DAPI in blue. (A) Control, (B) OGD, (C) OGD + MSC (Scale bar = 100  $\mu$ m). (D) HGF and BDNF were secreted from all three different lots of UC-MSCs. (E) HGF neutralizing antibody and recombinant Human TrkB Fc chimera were used for inhibition of HGF and BDNF respectively. As a negative control, recombinant human IgG1 Fc was used. Abbreviation: NAb, neutralizing antibody

## **VI-11. UC-MSCs restore both mature and immature neurons after OGD injury**

Under control conditions, both immature (GAP-43-positive; red) and mature (MAP-2-positive; green) neurons could be observed (Figure 19A). After OGD injury, neurites appeared diminished in length, and the number of cells positive for GAP-43 was reduced (Figure 19B). Co-culture with UC-MSCs maintained the mature neurons with long neurites to some extent, and increased the number of GAP-43-positive immature neurons (Figure 19C). Addition of NAbs reduced the UC-MSC-mediated improvement (Figure 19D-F). Quantitative analysis of GAP-43 expression revealed a significant decrease in the OGD compared to the control group, and that co-culture with UC-MSCs significantly improved GAP-43 expression relative to levels observed in the OGD group. On the other hand, addition of NAbs tended to decrease the expression of GAP-43 (Figure 19G). The length of neurites identified by immunofluorescence with MAP-2 was significantly shortened in the OGD relative to the control group, and co-culture with UC-MSCs significantly improved neurite outgrowth length. The addition of anti-HGF + BDNF NAbs significantly reduced neurite length after OGD (Figure 19H). Interestingly the effects of GAP-43 expression and neurite length were reverted partially by the addition of HGF and BDNF NAbs, and there was no synergistic effect by the addition of them.

**Figure19. Inhibition of HGF and BDNF decreases mature neurons and immature growing neurons after OGD**



Immature growing neurons were stained with GAP-43 in red and mature neurons were stained with MAP2 in green. (A) Control, (B) OGD, (C) OGD + MSC, (D) OGD + MSC + HGF NAb, (E) OGD + MSC + BDNF NAb, (F) OGD + MSC + HGF NAb + BDNF Nab (Scale bar = 100 μm). (G) Western blotting of GAP-43 expression and quantitative analysis of GAP-43 expression. β-tubulin was used as an internal control. (H) Quantitative analysis of neurites outlength. The data shown are representative of three independent experiments. \*\*p < 0.01

compared to Control group, and ##  $p < 0.01$ , #  $p < 0.05$  compared to OGD group.  
Abbreviation: NAb, neutralizing antibody.

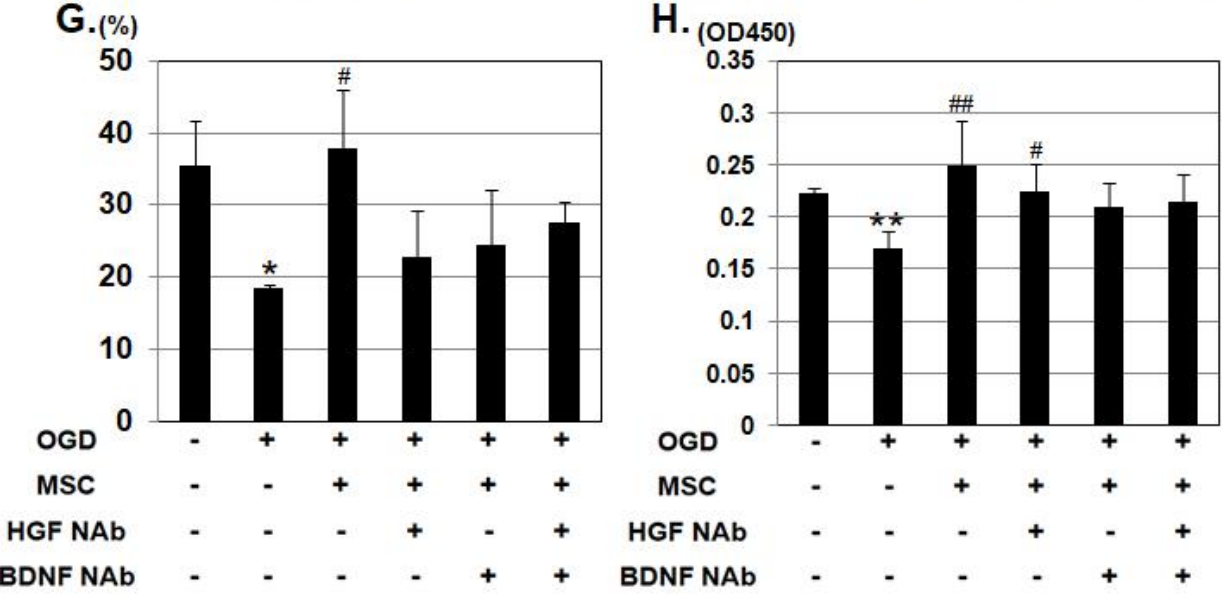
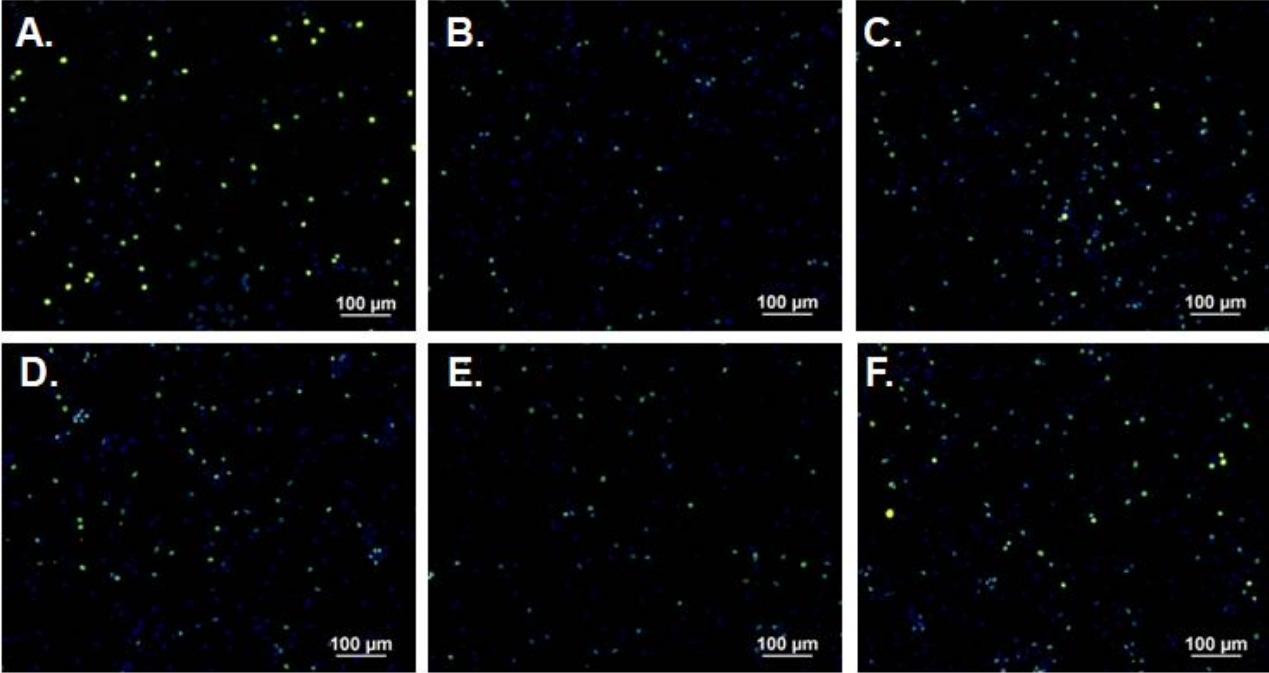
## **VI-12. UC-MSCs support mitosis of neurons after OGD with anti-apoptotic effect**

To investigate the effect of HGF and BDNF on cell proliferation, cortical neurons were stained with the mitotic marker, anti-histone H3, and counterstained with DAPI (Figure 20A). In the OGD group, the number of histone H3-positive cells decreased, whereas this reduction was restored in neurons co-cultured with UC-MSCs (Figure 20B-C). Addition of NAbs, however, attenuated this recovery (Figure 20D-F). Quantitative analysis revealed a significantly higher number of proliferating histone H3-positive cells in neurons co-cultured with UC-MSCs compared to neurons in the OGD group, whereas addition of NAbs to the OGD+MSC group decreased the amount of mitotic cells (Figure 20G). On the other hand, BrdU incorporation into neurons was reduced significantly in the OGD group. Co-culture with UC-MSCs significantly increased BrdU incorporation post-OGD (Figure 20H); however, the effect was not attenuated by the addition of NAbs.

Next, I examined the effect of HGF and BDNF on neuronal apoptosis/necrosis after OGD using FLICA labeling. We identified four populations of cells: living (FLICA-, PI-); early apoptotic (FLICA+, PI-); late apoptotic (FLICA+, PI+); and necrotic (FLICA-, PI+) (Figure 21A-G). Quantitative analysis of the ratio of apoptotic and necrotic cells to total cells revealed more apoptotic/necrotic cells in the OGD group compared to the control group. This analysis also demonstrated that co-culture with UC-MSCs reduced the number of cortical neurons displaying signs of apoptosis and necrosis post-OGD. This improvement was

attenuated by the addition of anti-BDNF or, especially, anti-HGF NAbs (Figure 21H), although no synergistic effect was observed in the group where both NAbs were added to the culture media.

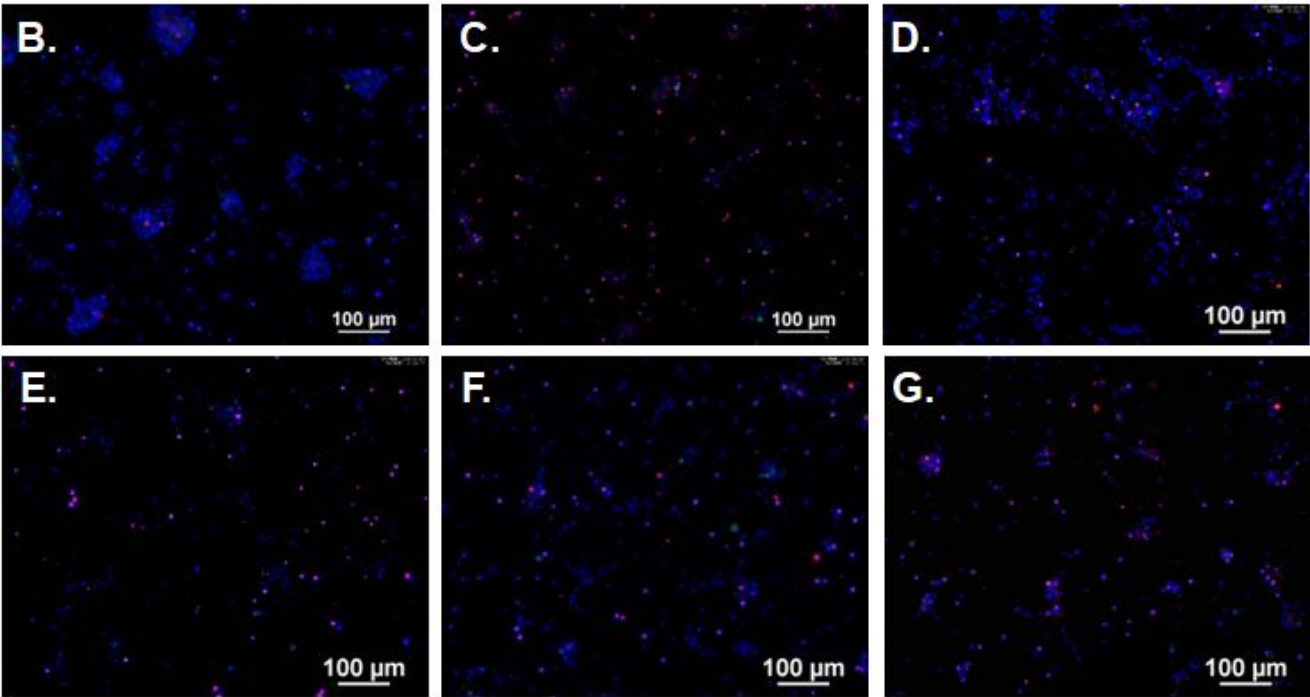
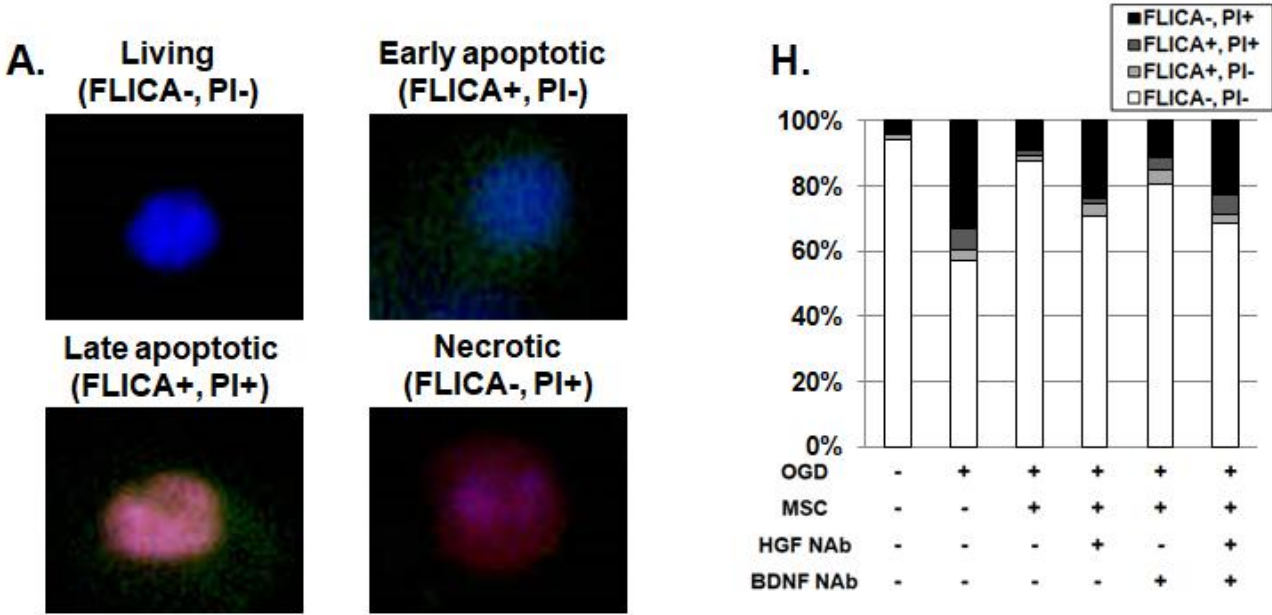
**Figure20. Inhibition of HGF and BDNF attenuates proliferation of neurons after OGD**



Mitotically proliferating neurons were stained with Histone H3 in green, counterstained with DAPI in blue. (A) Control, (B) OGD, (C) OGD + MSC, (D) OGD + MSC + HGF NAb, (E) OGD + MSC + BDNF NAb, (F) OGD + MSC + HGF NAb + BDNF Nab (Scale bar = 100 μm). (G) Quantitative analysis of the ratio of the number of Histone H3 positive cells to the total number of cells. (H) BrdU incorporation into proliferating neurons was measured and compared between six groups. \*\*p < 0.01, \*p < 0.05 compared to Control group, and ## p < 0.01, # p < 0.05 compared to OGD group. Abbreviation: NAb, neutralizing antibody.

**Figure21. Inhibition of HGF and BDNF increases apoptosis and necrosis of neurons**

after OGD



(A) The proportion of apoptotic and necrotic neurons after OGD using FLICA labeling. Four populations of cells were identified; living (FLICA-, PI-); early apoptotic (FLICA+, PI-); late apoptotic (FLICA+, PI+); and necrotic (FLICA-, PI+). Cell nuclei were counter-stained with Hoechst 33342. (B) Control, (C) OGD, (D) OGD + MSC, (E) OGD + MSC + HGF NAb, (F) OGD + MSC + BDNF NAb, (G) OGD + MSC + HGF NAb + BDNF Nab (Scale bar =

100  $\mu\text{m}$ ). (H) Quantitative analysis of the ratio of the number of apoptotic and necrotic cells to the total number of cells. Abbreviation: NAb, neutralizing antibody.

## VII. Discussion

Neonatal brain injuries during the perinatal period result in cerebral palsy that doesn't have radical therapies once it has manifested. Recent advances of regenerative therapies give us encouraging expectations in treating cerebral palsy. Perinatal brain damage that causes cerebral palsy includes (1) HIE, (2) IVH, and (3) PVL etc.

Hypothermia therapy has been widely applied to HIE, but its efficacy rate is 1 in 8 to 9 children who undergo the procedure, which means that it is not a perfect treatment by any means[52]. As a result of accumulating short-term prognoses of HIE children between 2012 to 2014 by the Japan Society of Perinatal and Neonatal Medicine, to which the authors belong, it was revealed that every year there is a 2 to 3% mortality rate prior to being discharged, around 10% of infants being discharged with respiratory apparatus, and about 20% of infants being discharged with tube feeding, and these short-term prognoses did not fall during these 3 years[53]. In recent years, Cotten et al. from Duke University in the United States reported that intravenous injection of autologous umbilical cord blood resulted in a greater number of cases developing a Bayley III score  $\geq 85$  in the surviving cases, compared to only hypothermia therapy ( $p = 0.05$ )[54]. Even in Japan, a multicenter clinical trial of autologous umbilical cord blood stem cell therapy for neonatal encephalopathy has been carried out ("Autologous Cord Blood Cell Therapy for Neonatal Hypoxic Ischemic Encephalopathy (HIE)" NIH ClinicalTrials.gov: NCT02256618). Although this treatment is a highly safe cell

therapy, at the time of birth of an infant with neonatal encephalopathy, both the mother and the child are in an imminent state, it is often the case that a sufficient amount of the umbilical cord blood cannot be collected in an aseptic manner. Furthermore, while many cases of neonatal encephalopathy occur in out-of-hospital births, such cases are out of the scope of this clinical study. Cord blood sampling is often difficult, IVH and PVL are excluded, and its effect is limited. Therefore, cell therapy is expected as a new alternative treatment.

IVH is bleeding that occurs inside the ventricle or brain parenchyma due to breakdown of blood vessels surrounding the ventricle or in the choroid plexus, and although common in preterm infants (under 36 weeks gestation), it is also seen in regular term infants. In terms of the time of onset of bleeding in preterm infants, 50% of cases occurred within 24 hours after birth, 25% by 2 days of age, 15% by 3 days of age, which shows that a majority of events occur within 3 days of birth. Papile's classification[55] is often used to classify the severity of intraventricular hemorrhage in preterm infants (Grade I: Subependymal bleeding only, Grade II: Intraventricular hemorrhage without ventricular enlargement, Grade III: Intraventricular hemorrhage with ventricular enlargement, Grade IV: Intraventricular hemorrhage accompanied by intraparenchymal hemorrhage). With regards to the frequency of IVH in preterm infants, Fanaroff et al. reported that IVH Grade I and II were seen in 15%, and Grade III and IV were seen in 12% of the 18,153 cases of extreme low-weight infants at birth born between 1997 and 2002[56]. Furthermore, in the large-scale NICU multicenter

investigation that was being carried out in Japan by the Neonatal Research Network, it was suggested that out of the 2,145 cases of newborns in 2003 with extreme-low weight at birth, IVH occurred in 13% of them, of which 7% accounted for IVH events with a severity of Grade III or Grade IV by the Papile classification[57]. After onset, systemic management such as coagulation factor supplementation, treatment of DIC, fresh frozen plasma, concentrated erythrocytes, platelet transfusion etc. are performed. Cerebral ventricular drainage may be necessary when a patient develops and has advanced post-hemorrhage hydrocephalus. It is very important to prevent IVH, because there are no effective treatments in the event that it develops.

PVL is an ischemic brain lesion occurring in the white matter around the ventricle, and because the development of blood vessels from the ventricle side is delayed and the formation of glia is also immature, decreases in cerebral blood flow make it easier for ischemic tissue necrosis to occur, and although this is common in preterm infants, it is also seen in regular term infants[58]. As risk factors, prenatal factors that can be highlighted include fetal distress, twin-to-twin transfusion syndrome, fetal growth restriction (FGR) and placenta previa, factors at the time of birth include neonatal asphyxiation, maternal bleeding that required emergency caesarean section, while factors after birth include apneic attack with bradycardia, sepsis, hypocapnia and patent ductus arteriosus. In the large-scale NICU multicenter investigation that was carried out by the Neonatal Research Network, 4% of the

2,145 cases of extreme low-weight infants born in 2003 had PVL[57]. They were diagnosed with either periventricular echodensities (PVE) or cystic PVL with a diameter of 3 mm or greater by head ultrasonography performed 7 days after birth, and head CT and MRI were used after the neonatal period. Because it is a post-ischemic lesion, there is no radical therapy, and rehabilitation etc. is performed from an early stage.

Human UC-MSCs have been reported for their self-renewal capacity and multi-lineage differentiation potential [59-61], including differentiation into the neurogenic lineage, as reported previously [6, 62]. The potency of neurogenic differentiation derived from autologous or allogeneic UC-MSCs is an attractive system to treat patients with inborn cerebral palsy. Accordingly, several neurogenic differentiation protocols—particularly those for neural and glial cells—are under investigation, including those for neurosphere formation [63]. Here, I obtained whole UC-derived MSCs that retained their competency for neurogenic differentiation and migration on culturing in conditions favorable for neurosphere formation. Furthermore, expression of the stemness markers was also induced in UC-MSC-neurospheres. The neurosphere formation technique was first reported by Kabos et al. in 2002 [64]. Neurospheres are defined as free-floating spherical aggregates of neural stem cells that can proliferate in culture but retain their capacity to differentiate in neurons or glial cells [65].

The UC tissue contains various sources of MSCs that are competent to undergo neurogenic differentiation. In addition, MSCs-derived from Wharton's jelly—which is mainly

composed of UC extracellular matrix—can also form neurospheres [66, 67]. Karahuseyinoglu et al. demonstrated that cultured human UC-derived cells contain two distinct populations, type 1 and type 2, which may correspond to perivascular cells and intervascular cells, respectively. However, no differences were found between the two regarding neuronal differentiation *in vitro* [68].

It is still controversial whether the whole or only some of this cellular compartment is superior in its proliferation, differentiation, and immunosuppressive capacities [69, 70], and all express the MSC markers CD105, CD90, and CD73 [71]. According to previous reports [72-74], I speculated that removing the artery and veins from the UC Wharton's jelly may limit the stemness of these MSCs. Therefore, MSCs were isolated from whole UC using the explant method, which is simple and does not require digestive enzymes.

The component cell number and the size of UC-MSC-neurospheres were consistent with those previously derived from BM-MSCs [75]. The UC-MSC-neurospheres were composed of approximately  $1 \times 10^4$  cells, meaning that the cells did not proliferate during the formation of neurospheres cultured in low adherence culture plates, yet they regained this potential after transfer to standard coated plates.

I also studied the effect of neurosphere formation on the neurogenic differentiation in UC-MSCs. The formation of neurospheres did not change the level of neural- and

glial-specific markers themselves and there were no significant differences between UC-MSCs and UC-MSC-neurospheres in the gene expression of *PAX6* and *MUSASHI1*, *GFAP*, and *MAP2*, as neural-progenitor, astrocyte, and mature neuron markers, by RT-PCR respectively. These molecules were induced to a greater extent in UC-MSC-neurospheres than UC-MSCs after culture in neurogenic differentiation medium. Both the induction of the molecules and the proportion of MAP-2- and Musashi-1-positive cells were higher in the differentiated UC-MSC-neurosphere and differentiated UC-MSC groups than in their undifferentiated counterparts. Interestingly, differentiated UC-MSC-neurospheres exhibited qualities of stem/progenitor cells, as well as mature neural and glial cells, whereas differentiated UC-MSCs only displayed those for stem/progenitor cells and mature neural cells. I also characterized the migrating cells from differentiated UC-MSC-neurospheres, and the cells exhibited surface markers of MSCs criteria. I assume that the cells migrating from differentiated UC-MSC-neurospheres exhibit neural markers while maintaining MSC characteristics, although the neurosphere may be consisted with the uneven cells.

Furthermore, the stemness markers *OCT4* [76, 77], *NANOG* [78], and *KLF4* [79] were highly expressed in the UC-MSC-neurospheres. Guo et al. reported that the spheroid culture of human MSCs increased their expression of these genes [80], and my results were consistent with this study. However, some reports emphasize that the heterogeneous cell populations in neurospheres can shuttle between quiescent and activated states, and even

more committed progenitors can revert back to a more primitive state [81] [82]. Although I could not distinguish the cells expressing *MAP2* from those expressing *OCT4*, the cells migrating from the neurosphere expressed an abundance of *MAP2* and *MUSASH1*. Moreover,  $\beta$ III-tubulin was expressed in UC-MSCs and UC-MSC-neurospheres, regardless of the induction of neurogenic differentiation seen in immunocytochemistry, immunoblotting and quantitative RT-PCR, although the precise reason remained unresolved. These results suggested that the neurosphere formation facilitate UC-MSCs dedifferentiation toward a higher hierarchy by expressing ES-like cell genes and thus the cells may acquire a greater capacity to differentiate into neural and glial cells, while UC-MSCs cannot differentiate into glial cells. The neurosphere formation might be similar to multilineage-differentiating stress enduring (Muse) cell maintenance [83, 84], although the neurospheres seemed to prefer neurogenic differentiation.

In addition, I investigated the respective effects of differentiation and dissociation on the migratory abilities of UC-MSC-neurospheres *in vitro*. I used glucose-depleted neuronal cell lines to induce UC-MSC-neurosphere migration to mimicking ischemia-damaged neural tissue [39]. As expected, the results showed the number of migratory UC-MSCs was higher in the glucose-depleted group than controls. Lambert et al. reported increased expression and secretion of neurotrophins such as nerve growth factor (NGF), brain-derived neurotrophic factor (BDNF), and neurotrophin-3 (NT-3) by optic nerve cells after culture in conditions that

mimic ischemia [85]. While these chemo-attractants from glucose-depleted neural cells might lead to the enhanced migration of UC-MSCs, I also found that non-neurogenic HeLa cells exhibited migratory capacity to these factors (data not shown). CXC chemokine receptor 4 (CXCR4), a chemokine receptor specific for stromal cell-derived factor 1  $\alpha$  (SDF1 $\alpha$ ), is highly expressed on specific stem cells, like neural stem cells. Previous studies demonstrated that increasing CXCR4 expression on MSCs enhance their homing ability to injured site [45, 86]. On the other hand, Ruster et al reported that P-selectin and VCAM-1/VLA-4 are important factor for binding of MSCs to endothelial cells [87]. Further studies are needed to analyze migration mechanisms of UC-MSCs.

Next, I investigated the restorative effects of UC-MSCs cultured with serum-free medium in the neonatal IVH model. IVH is a common complication in preterm neonates and is responsible for high mortality and subsequent disabilities such as cerebral palsy. However there are no effective therapies available for IVH at present. I first established an animal model of neonatal IVH treated with UC-MSCs. Two models have been reported to mimic clinical IVH in mice: the collagenase model, in which injected collagenase induces vessel rupture and induces intracerebral bleeding, and the autologous whole blood model, in which autologous blood is injected into brain directly [43]. Referencing the latter method, I have established a neonatal IVH model [31, 71] at postnatal day 5, which is roughly comparable to 24 to 26 week gestational age in the human brain [88, 89]. Concerning the route of injection,

many prior studies administered MSCs by direct injection to the brain [8, 42, 90-92].

However, I acknowledge that a real clinical situation may not allow the intraventricular injection of UC-MSCs because of potential complications for neonates. As for the dose of UC-MSCs for neonatal IVH model mice, the number of cells was determined with reference to previous reports using neonatal brain damage model mice [90, 93, 94], and I decided the dose so that pulmonary infarction resulting from intravenous injection does not occur. It is necessary to decide the dose or the number of administrations in order to ensure safety and effectiveness of UC-MSCs administration clinically.

In the study, I successfully generated an IVH model, as indicated by ventricular dilatation confirmed by brain MRI, and an intravenous injection model with UC-MSCs. Ventricular dilatation might have progressed in the same mechanism as the following posthemorrhagic hydrocephalus (PHH) after IVH which occurs especially in extremely preterm infants [95]. Although the ventricular dilatation was not diminished in size in UC-MSC-administered groups compared with the IVH group within short-term observation, UC-MSCs improved activity in both locomotor distance and number of times rearing in the open field test. Ahn et al. reported that CB-derived MSC intraventricular transplantation for severe IVH significantly attenuated the post-hemorrhagic hydrocephalus, contrary to my findings [42]. The contradicting results of MRI and motor activity tests might be due to the different observation period and route of administration. Therefore, there is a possibility that

the dilatation in my system might be ameliorated in the long term. Within a short-term observation period, similar to that in the clinical setting, I observed the improvement of motor abilities even though ventricular dilatation was not improved.

In the open field test, UC-MSc-administered groups showed improved activity in both distance traveled and number of times in rearing. However, there were no significant differences between groups in hind-stride length and hind-base width in the footprint analysis. These results may suggest that IVH surgery affects locomotor activity rather than motor coordination and synchrony because it caused bilateral ventricular dilatation. Among UC-MSc groups, the IVH + UC-MScs (RM) group exhibited the most significant improvement compared to the IVH group in the open field test. From these results, I inferred that UC-MScs cultured with RM were equivalent to those cultured with MEM in the IVH treatment model.

In the damaged tissue in the IVH model, previous studies showed that reactive gliosis, also known as glial scar formation, was mainly characterized by the proliferation of microglia and astrocytes [43], as well as astrocytic hypertrophy occurring after injury in the central nervous system [43, 96, 97]. These pathological changes after IVH resulted in white matter injury demonstrated by MBP reduction and a large number of apoptotic cells in periventricular tissue [42, 43, 49-51, 98, 99]. As well, in my study, it is considered that destruction of periventricular white matter, and infiltration of neutrophil and macrophage have

occurred, followed by reactive gliosis and hypomyelination. I demonstrated that intravenous injection of UC-MSCs could attenuate periventricular reactive gliosis, hypomyelination, and periventricular cell death as potential mechanisms for behavioral improvement.

In order to investigate factors underlying pathological and functional improvement, I examined substances secreted from UC-MSCs in IVH mice. I found that elevated human BDNF and HGF were detected not only in the sera, but also in CSF and brain tissue of UC-MSC-administered mice, while NGF was not secreted in any group. BDNF and HGF have been reported to be able to permeate across blood brain barrier (BBB) [100, 101]. In addition, it has been reported that IVH induces BBB disruption and increased BBB permeability [102]. Therefore IVH surgery in my study might induce increased permeability of BBB followed by elevation of BDNF and HGF although I couldn't detect them in all mice treated with UC-MSCs in my hands. Guo et al. reported that conditioned medium of UC-MSCs exhibited high concentration of BDNF and HGF, while NGF was secreted at a low level [103], consistent with my study. As for mechanisms that UC-MSCs relieved gliosis and hypomyelination, BDNF has been reported to improve hypomyelination via Erk phosphorylation or TrkB signaling [104, 105]. And also HGF has been reported to influence the development and growth of oligodendrocytes, as well as the proliferation of myelin-forming Schwann cells [106]. In addition, Kadoyama et al. indicated that HGF reduces gliosis by suppressing MCP-1 induction [107]. These mechanisms of BDNF and HGF

might alleviate gliosis and hypomyelination observed after IVH. There have been several reports of secretion of BDNF and HGF from UC-MSCs *in vitro* but not yet *in vivo*. To my knowledge, this is the first study showing that administered UC-MSCs can secrete trophic factors, BDNF and HGF, in newborn mice after IVH and can attenuate periventricular reactive gliosis, hypomyelination, and periventricular cell death. However, this study is limited by the antibodies available to detect relevant factors. Furthermore, my study system is xenogeneic involving human and mouse, and other factors may be elevated in an allogeneic system.

With regard to the migration and elimination of administered UC-MSCs, IVIS showed that UC-MSCs steadily spread to the head and neck, with the signal peaking 3 days after UC-MSC injection. Similarly, genomic DNA PCR showed that the Alu gene was detected one day after injection mostly in brain and lung, and immunohistochemistry revealed that UC-MSCs migrated in brain. Previously, I reported the migration ability of UC-MSCs towards injured neural cells with glucose depletion [108], and *in vivo* results also suggest the migration ability of UC-MSCs toward the injured brain. UC-MSCs were undetectable in IVIS, Alu PCR, and immunohistochemistry 3 weeks after injection. It is appreciated that the administered MSCs should be eliminated to reduce the long-term risk of malignant transformation, although MSCs have been reported to be relatively safe in terms of genomic instability showing progressive growth arrest and entered senescence without evidence of

transformation either *in vitro* or *in vivo* [109-111]. These results suggest that amelioration of neuronal injury followed by functional improvement might result from secretion of trophic factors such as BDNF and HGF rather than neuronal differentiation and eternal cell replacement by UC-MSCs.

Finally I investigated whether HGF and BDNF secreted from UC-MSCs contribute to neurogenesis, proliferation and viability in injured nerve system *in vitro*. According to the study done by Guo et al. paracrine factors caused by UC-MSCs are important in peripheral nerve repair. They showed that neurotrophic factors, such as BDNF, HGF, glial-derived neurotrophic factor (GDNF), neurotrophin-3 (NT-3), and basic fibroblast growth factor (bFGF) are highly expressed in UC-MSCs cultured medium, while some other factors (nerve growth factor (NGF)- $\beta$  and vascular endothelial growth factor (VEGF) were secreted at low concentrations [103]. Martins et al. also revealed UC-MSCs secretome can promote axonal growth in neurons and this effect is mediated by BDNF secreted from UC-MSCs [36]. In previous studies so far, the questions remain how much HGF and BDNF secreted from UC-MSCs contribute to neurogenesis and viability in injured nerve system. Therefore I investigated the effect of HGF and BDNF alone or both of them secreted from UC-MSCs on neurogenesis and viability of injured neurons.

I first confirmed constitutive secretion of HGF and BDNF from UC-MSCs, and inhibition of them by neutralizing antibodies. HGF and BDNF were secreted from all lots of

UC-MSCs consistent with a previous report [103]. The concentration of HGF and BDNF in UC-MSCs were 0.079 times and 0.89 times those of SH-SY5Y cells respectively. However, the level of concentration varied between lots of UC-MSCs. In this regard, the differences between lots of UC-MSCs may result from differences in the background such as gestational weeks, maternal information, and status of babies at birth etc. Regarding to inhibition of HGF and BDNF, HGF neutralizing antibody and recombinant Human TrkB Fc chimera used in previous reports [36, 46] properly reduced the concentration of HGF and BDNF in my experiment.

In this study, I successfully generated an *in vitro* OGD model of primary cortical -neurons, as indicated by shortened neurites, a reduction in the number of network-forming neurites, fewer developing neurons, decreased cell proliferation, and increased apoptosis/necrosis. Co-culture with UC-MSCs was sufficient to maintain the number of MAP2-positive mature neurons showing extended neurites and cluster formations, whereas HGF and BDNF NAbs significantly attenuated the restorative effect of UC-MSCs on neurite elongation. These phenomena were also supported by the anti-apoptotic effect of UC-MSCs observed in the FLICA experiment. Furthermore, the number of GAP-43-positive cells appeared significantly increased in the UC-MSC co-culture group, suggesting the generation of immature, developing neurons. Consistent with this result, an increase in the number of histone H3-positive mitotic cells, as well as an enhancement in the amount of BrdU

incorporation, were observed in UC-MSC co-cultured cells compared to cells in the OGD group. The restorative effects induced by UC-MSCs on GAP-43- and histone H3-positive labeling were reverted by the addition of HGF and BDNF NAbs. Interestingly, BrdU incorporation was not influenced by the addition of these NAbs, although the reason for this discrepancy remains unresolved. HGF and BDNF NAbs partially reverted the restorative effects of UC-MSCs; however, in our hands, there was no synergistic effect when both NAbs were simultaneously added to the culture medium. Although the addition of HGF and BDNF NAbs were partially effective in blocking the neuroprotective actions of UC-MSCs, restorative effects could still be observed. This suggests the possible existence of other UC-MSC-secreted trophic factors.

HGF is a multi-functional growth factor originally reported as a potent mitogen for mature parenchymal hepatocytes in primary culture, and is reported to play an important role for tissue regeneration including nervous system. It has been reported that HGF binds a tyrosine kinase receptor encoded by the c-Met, and that HGF and c-Met are expressed in both of adult and fetal central nervous system [112, 113]. Activation of the downstream pathways such as phosphatidylinositol 3-kinase/Akt pathway, MAP-kinase pathway, and the signal transducers and activators of transcription 3 (STAT3) pathway leads to neurorestorative effects including anti-apoptosis and neurogenesis [112-114]. Liu X et al. reported the neuroprotective effect of UC-MSCs infected with adenovirus expressing HGF gene on the

Parkinson's disease model via promotion of damaged cells regeneration [115]. These previous reports support the important role of HGF for neurogenesis and cell viability, and in this study as well, inhibition of HGF attenuated the effectiveness of neurogenesis, cell proliferation and viability.

With regard to BDNF, also known as a second neurotrophic factor to be characterized, after NGF and before neurotrophin-3, it is expressed in adult and developing brain as well as HGF, and plays a key role in the proliferation, survival and differentiation of neurons [116-118]. BDNF binds to tropomyosin-related kinase (Trk) family of receptor tyrosine kinases (TrkA, TrkB and TrkC) and activates phosphatidylinositol 3-kinase/Akt pathway and MAP-kinase pathway. In addition, each neurotrophin activates p75 neurotrophin receptor (p75NTR), and activation of p75NTR results in activation of the nuclear factor-kB (NF-kB). These signaling pathways lead to activation of prosurvival genes and prodifferentiation genes [119]. In this study, inhibition of BDNF decreased the extent of neurogenesis and cell viability, and this phenomenon might result from the key role of BDNF mentioned above.

In order to further deepen the research, I knocked down HGF or BDNF or both of them by shRNA from Dharmacon (SMARTvector™) using lentiviral vector system and performed cell sorting. However knocked-down UC-MSCs did not adhere sufficiently to culture dish and the remaining adhered cells did not proliferate at all and gradually floated and died (data not shown). These results indicate that knocking down of HGF or BDNF is fatal for

UC-MSCs and that they are essential for cell proliferation and survival.

The results in this study indicate that HGF and BDNF secreted from UC-MSCs contribute to neurogenesis, cell proliferation and survival in injured nerve system, and that there are also other factors secreted from UC-MSCs which contribute to neurogenesis, proliferation and viability of neurons.

The cell therapy cannot be replaced with the administration of the trophic factors for the purpose to treat such complicated disease, cerebral palsy. The reasons that cell therapy is more effective than administration of specific growth factors such as HGF and BDNF are (1) the migratory ability of the MSCs to the site of injury and (2) the possibility of a existence of other trophic factors other than BDNF and HGF. MSCs have an ability of migration/homing to damaged site of the body suggested by our experiments results and previous studies [45, 86, 120]. Therefore, in order for the trophic factors to reach the site of injury, it might be more effective that MSCs migrate to the site and secrete trophic factors than systemic administration of trophic factors themselves. In addition, inhibition experiment *in vitro* suggested the presence of other important neurotrophic factors secreted from UC-MSCs. From these reasons, it was considered that UC-MSCs administration might be more effective than administration of specific trophic factors alone.

Further studies are needed to examine the elevation of cytokines after IVH and determine the dose protocol of UC-MSC administration. The development of IVH results in

an inflammatory response [121], and it has been reported that UC-MSCs have immunomodulatory properties [5]. Therefore, UC-MSCs may play a key role in management of these inflammatory cytokines. Inflammatory cytokines after IVH and the optimal timing and number of doses of UC-MSCs administration are now undergoing further study. As another problem, the concentrations of secreted HGF and BDNF demonstrated variability that was dependent on UC-MSC lot. Lot-to-lot variation in these secreted neurotrophic factors is an important issue considering their potential for clinical application.

Recently, cell therapies with various sources, including cord blood, BM, umbilical cord, amnion, and adipose tissue, in neonatal brain injuries that may cause cerebral palsy have been reported in animal models. In the clinic, Kurtzberg et al. reported the use of autologous cord blood for babies with infant cerebral palsy [54], but autologous cord blood collection requires refined technique, and it is occasionally difficult to collect a great enough volume of cord blood. Although the use of autologous UC-MSCs requires long-term quality and safety assessment until injection, recent clinical trials with off-the-shelf UC-MSCs from an allogeneic third party are encouraging for their safety and efficacy without any serious adverse events [16] [17] [18]. Most recently, Wang et al. [19] reported the efficacy of UC-MSC transplantation on the motor function of identical twins with cerebral palsy. Eight pairs of twins showed significant improvement of Gross Motor Function Measures at 1 and 6 months after UC-MSC transplantation. These clinical results encourage us to facilitate

allogeneic third-party UC-MSc therapy for IVH treatment. Notably, the intravenous injection of UC-MSCs in IVH babies is to be implemented more in clinic. In addition, supplemented FBS in the medium with which UC-MSCs are cultured is arguably the most critical safety factor in clinical situation because of xenogeneic antigens and possible infections including BSE. Therefore, lower antigenic and safer medium is preferred for clinical use.

In conclusion, I demonstrated that UC-MSCs have neurogenic differentiation potential, neurosphere formation ability and migration ability towards injured neuronal cells *in vitro*, and that UC-MSCs cultured with RM medium migrate towards brain with intravenous administration, secreting BDNF and HGF, and play a significant role in attenuating IVH-induced brain injuries. In addition, I revealed UC-MSCs restore neurogenesis and cell viability of damaged primary fetal neurons and that these findings were attenuated by inhibition of BDNF and HGF *in vitro*.

These results suggest that UC-MSCs ameliorate neuronal injury followed by functional improvement by secretion of neurotrophic factors such as BDNF and HGF rather than neuronal differentiation and eternal cell replacement, and that intravenous injection of UC-MSCs may be feasible treatment for neonatal brain injuries.

These works were published in *Cytotherapy* on 18th February 2016, entitled “Neurosphere formation enhances the neurogenic differentiation potential and migratory ability of umbilical cord-mesenchymal stromal cells”, and in *Neuroscience* on 11th May 2017, entitled “Intravenous injection of umbilical cord-derived mesenchymal stromal cells attenuates reactive gliosis and hypomyelination in a neonatal intraventricular hemorrhage model”.

## VIII. References

1. Dixon BJ, Reis C, Ho WM, Tang J, Zhang JH. Neuroprotective Strategies after Neonatal Hypoxic Ischemic Encephalopathy. *Int J Mol Sci* 2015;16(9):22368-401.
2. Kristian T. Metabolic stages, mitochondria and calcium in hypoxic/ischemic brain damage. *Cell Calcium* 2004;36(3-4):221-33.
3. Mendonca MV, Larocca TF, de Freitas Souza BS, et al. Safety and neurological assessments after autologous transplantation of bone marrow mesenchymal stem cells in subjects with chronic spinal cord injury. *Stem Cell Res Ther* 2014;5(6):126.
4. Nagamura-Inoue T, Mukai T. Umbilical Cord is a Rich Source of Mesenchymal Stromal Cells for Cell Therapy. *Curr Stem Cell Res Ther* 2016;11(8):634-42.
5. He H, Nagamura-Inoue T, Takahashi A, et al. Immunosuppressive properties of Wharton's jelly-derived mesenchymal stromal cells in vitro. *Int J Hematol* 2015;102(3):368-78.
6. Leite C, Silva NT, Mendes S, et al. Differentiation of human umbilical cord matrix mesenchymal stem cells into neural-like progenitor cells and maturation into an oligodendroglial-like lineage. *PLoS One* 2014;9(10):e111059.
7. Hsieh JY, Wang HW, Chang SJ, et al. Mesenchymal stem cells from human umbilical cord express preferentially secreted factors related to neuroprotection, neurogenesis, and angiogenesis. *PLoS One* 2013;8(8):e72604.

8. Ding DC, Shyu WC, Chiang MF, et al. Enhancement of neuroplasticity through upregulation of beta1-integrin in human umbilical cord-derived stromal cell implanted stroke model. *Neurobiol Dis* 2007;27(3):339-53.
9. Cheng Q, Zhang Z, Zhang S, et al. Human umbilical cord mesenchymal stem cells protect against ischemic brain injury in mouse by regulating peripheral immunoinflammation. *Brain Res* 2015;1594:293-304.
10. Wu KH, Chan CK, Tsai C, et al. Effective treatment of severe steroid-resistant acute graft-versus-host disease with umbilical cord-derived mesenchymal stem cells. *Transplantation* 2011;91(12):1412-6.
11. Fu Y, Wang Q, Zhou J, et al. Reduced intensity conditioning and co-transplantation of unrelated peripheral stem cells combined with umbilical cord mesenchymal stem/stroma cells for young patients with refractory severe aplastic anemia. *Int J Hematol* 2013;98(6):658-63.
12. Wang H, Wang Z, Zheng X, et al. Hematopoietic stem cell transplantation with umbilical cord multipotent stromal cell infusion for the treatment of aplastic anemia--a single-center experience. *Cytotherapy* 2013;15(9):1118-25.
13. Si Y, Yang K, Qin M, et al. Efficacy and safety of human umbilical cord derived mesenchymal stem cell therapy in children with severe aplastic anemia following allogeneic hematopoietic stem cell transplantation: a retrospective case series of 37 patients. *Pediatr*

Hematol Oncol 2014;31(1):39-49.

14. Wu Y, Wang Z, Cao Y, et al. Cotransplantation of haploidentical hematopoietic and umbilical cord mesenchymal stem cells with a myeloablative regimen for refractory/relapsed hematologic malignancy. *Ann Hematol* 2013;92(12):1675-84.

15. Zhu L, Wang Z, Zheng X, et al. Haploidentical hematopoietic stem cell transplant with umbilical cord-derived multipotent mesenchymal cell infusion for the treatment of high-risk acute leukemia in children. *Leuk Lymphoma* 2015;56(5):1346-52.

16. Dongmei H, Jing L, Mei X, et al. Clinical analysis of the treatment of spinocerebellar ataxia and multiple system atrophy-cerebellar type with umbilical cord mesenchymal stromal cells. *Cytotherapy* 2011;13(8):913-7.

17. Jin JL, Liu Z, Lu ZJ, et al. Safety and efficacy of umbilical cord mesenchymal stem cell therapy in hereditary spinocerebellar ataxia. *Curr Neurovasc Res* 2013;10(1):11-20.

18. Wang S, Cheng H, Dai G, et al. Umbilical cord mesenchymal stem cell transplantation significantly improves neurological function in patients with sequelae of traumatic brain injury. *Brain Res* 2013;1532:76-84.

19. Wang X, Hu H, Hua R, et al. Effect of umbilical cord mesenchymal stromal cells on motor functions of identical twins with cerebral palsy: pilot study on the correlation of efficacy and hereditary factors. *Cytotherapy* 2015;17(2):224-31.

20. Li X, Hu YD, Guo Y, et al. Safety and efficacy of intracoronary human umbilical

cord-derived mesenchymal stem cell treatment for very old patients with coronary chronic total occlusion. *Curr Pharm Des* 2015;21(11):1426-32.

21. Zhao XF, Xu Y, Zhu ZY, Gao CY, Shi YN. Clinical observation of umbilical cord mesenchymal stem cell treatment of severe systolic heart failure. *Genet Mol Res* 2015;14(2):3010-7.

22. Musialek P, Mazurek A, Jarocha D, et al. Myocardial regeneration strategy using Wharton's jelly mesenchymal stem cells as an off-the-shelf 'unlimited' therapeutic agent: results from the Acute Myocardial Infarction First-in-Man Study. *Postepy Kardiol Interwencyjnej* 2015;11(2):100-7.

23. Can A, Ulus AT, Cinar O, et al. Human Umbilical Cord Mesenchymal Stromal Cell Transplantation in Myocardial Ischemia (HUC-HEART Trial). A Study Protocol of a Phase 1/2, Controlled and Randomized Trial in Combination with Coronary Artery Bypass Grafting. *Stem Cell Rev* 2015.

24. Shi M, Zhang Z, Xu R, et al. Human mesenchymal stem cell transfusion is safe and improves liver function in acute-on-chronic liver failure patients. *Stem Cells Transl Med* 2012;1(10):725-31.

25. Xue HL, Zeng WZ, Wu XL, et al. Clinical therapeutic effects of human umbilical cord-derived mesenchymal stem cells transplantation in the treatment of end-stage liver disease. *Transplant Proc* 2015;47(2):412-8.

26. Cai J, Wu Z, Huang L, et al. Cotransplantation of bone marrow mononuclear cells and umbilical cord mesenchymal stem cells in avascular necrosis of the femoral head. *Transplant Proc* 2014;46(1):151-5.
27. Guan LX, Guan H, Li HB, et al. Therapeutic efficacy of umbilical cord-derived mesenchymal stem cells in patients with type 2 diabetes. *Exp Ther Med* 2015;9(5):1623-30.
28. Wang D, Zhang H, Liang J, et al. Allogeneic mesenchymal stem cell transplantation in severe and refractory systemic lupus erythematosus: 4 years of experience. *Cell Transplant* 2013;22(12):2267-77.
29. Mori Y, Ohshimo J, Shimazu T, et al. Improved explant method to isolate umbilical cord-derived mesenchymal stem cells and their immunosuppressive properties. *Tissue Eng Part C Methods* 2015;21(4):367-72.
30. Xiang J, Tang J, Song C, et al. Mesenchymal stem cells as a gene therapy carrier for treatment of fibrosarcoma. *Cytotherapy* 2009;11(5):516-26.
31. Xue M, Balasubramaniam J, Buist RJ, Peeling J, Del Bigio MR. Periventricular/intraventricular hemorrhage in neonatal mouse cerebrum. *J Neuropathol Exp Neurol* 2003;62(11):1154-65.
32. Kienstra KA, Freysdottir D, Gonzales NM, Hirschi KK. Murine neonatal intravascular injections: modeling newborn disease. *J Am Assoc Lab Anim Sci* 2007;46(6):50-4.

33. Heck DH, Zhao Y, Roy S, LeDoux MS, Reiter LT. Analysis of cerebellar function in Ube3a-deficient mice reveals novel genotype-specific behaviors. *Hum Mol Genet* 2008;17(14):2181-9.
34. Kim ES, Ahn SY, Im GH, et al. Human umbilical cord blood-derived mesenchymal stem cell transplantation attenuates severe brain injury by permanent middle cerebral artery occlusion in newborn rats. *Pediatr Res* 2012;72(3):277-84.
35. Liu Y, Zhang Y, Lin L, et al. Effects of bone marrow-derived mesenchymal stem cells on the axonal outgrowth through activation of PI3K/AKT signaling in primary cortical neurons followed oxygen-glucose deprivation injury. *PLoS One* 2013;8(11):e78514.
36. Martins LF, Costa RO, Pedro JR, et al. Mesenchymal stem cells secretome-induced axonal outgrowth is mediated by BDNF. *Sci Rep* 2017;7(1):4153.
37. Baldassarro VA, Marchesini A, Giardino L, Calza L. Vulnerability of primary neurons derived from Tg2576 Alzheimer mice to oxygen and glucose deprivation: role of intraneuronal amyloid-beta accumulation and astrocytes. *Dis Model Mech* 2017;10(5):671-8.
38. Mukai T, Nagamura-Inoue T, Shimazu T, et al. Neurosphere formation enhances the neurogenic differentiation potential and migratory ability of umbilical cord-mesenchymal stromal cells. *Cytotherapy* 2016;18(2):229-41.
39. Czubowicz K, Cieslik M, Pyszko J, Strosznajder JB, Strosznajder RP. Sphingosine-1-Phosphate and Its Effect on Glucose Deprivation/Glucose Reload Stress: From

Gene Expression to Neuronal Survival. *Mol Neurobiol* 2014.

40. Agata H, Asahina I, Watanabe N, et al. Characteristic change and loss of in vivo osteogenic abilities of human bone marrow stromal cells during passage. *Tissue Eng Part A* 2010;16(2):663-73.

41. Dominici M, Le Blanc K, Mueller I, et al. Minimal criteria for defining multipotent mesenchymal stromal cells. The International Society for Cellular Therapy position statement. *Cytotherapy* 2006;8(4):315-7.

42. Ahn SY, Chang YS, Sung DK, et al. Mesenchymal stem cells prevent hydrocephalus after severe intraventricular hemorrhage. *Stroke* 2013;44(2):497-504.

43. Zhu W, Gao Y, Chang CF, et al. Mouse models of intracerebral hemorrhage in ventricle, cortex, and hippocampus by injections of autologous blood or collagenase. *PLoS One* 2014;9(5):e97423.

44. Chen D, Xia Y, Zuo K, et al. Crosstalk between SDF-1/CXCR4 and SDF-1/CXCR7 in cardiac stem cell migration. *Sci Rep* 2015;5:16813.

45. Wang Z, Wang Y, Wang Z, et al. Engineered Mesenchymal Stem Cells with Enhanced Tropism and Paracrine Secretion of Cytokines and Growth Factors to Treat Traumatic Brain Injury. *Stem Cells* 2015;33(2):456-67.

46. Brauer HA, Makowski L, Hoadley KA, et al. Impact of tumor microenvironment and epithelial phenotypes on metabolism in breast cancer. *Clin Cancer Res* 2013;19(3):571-85.

47. Casbas-Hernandez P, D'Arcy M, Roman-Perez E, et al. Role of HGF in epithelial-stromal cell interactions during progression from benign breast disease to ductal carcinoma in situ. *Breast Cancer Res* 2013;15(5):R82.
48. Abellaneda JM, Martinez-Alarcon L, Quereda JJ, et al. Validation of a quantitative polymerase chain reaction method for human Alu gene detection in microchimeric pigs used as donors for xenotransplantation. *Transplant Proc* 2015;47(1):132-5.
49. Gram M, Sveinsdottir S, Ruscher K, et al. Hemoglobin induces inflammation after preterm intraventricular hemorrhage by methemoglobin formation. *J Neuroinflammation* 2013;10:100.
50. Georgiadis P, Xu H, Chua C, et al. Characterization of acute brain injuries and neurobehavioral profiles in a rabbit model of germinal matrix hemorrhage. *Stroke* 2008;39(12):3378-88.
51. Chua CO, Chahboune H, Braun A, et al. Consequences of intraventricular hemorrhage in a rabbit pup model. *Stroke* 2009;40(10):3369-77.
52. Jacobs SE, Berg M, Hunt R, et al. Cooling for newborns with hypoxic ischaemic encephalopathy. *Cochrane Database Syst Rev* 2013;1:CD003311.
53. Tsuda K, Mukai T, Iwata S, et al. Therapeutic hypothermia for neonatal encephalopathy: a report from the first 3 years of the Baby Cooling Registry of Japan. *Sci Rep* 2017;7:39508.

54. Cotten CM, Murtha AP, Goldberg RN, et al. Feasibility of autologous cord blood cells for infants with hypoxic-ischemic encephalopathy. *J Pediatr* 2014;164(5):973-9 e1.
55. Papile LA, Burstein J, Burstein R, Koffler H. Incidence and evolution of subependymal and intraventricular hemorrhage: a study of infants with birth weights less than 1,500 gm. *J Pediatr* 1978;92(4):529-34.
56. Fanaroff AA, Stoll BJ, Wright LL, et al. Trends in neonatal morbidity and mortality for very low birthweight infants. *Am J Obstet Gynecol* 2007;196(2):147 e1-8.
57. Kusuda S, Fujimura M, Sakuma I, et al. Morbidity and mortality of infants with very low birth weight in Japan: center variation. *Pediatrics* 2006;118(4):e1130-8.
58. Kinney HC. The near-term (late preterm) human brain and risk for periventricular leukomalacia: a review. *Semin Perinatol* 2006;30(2):81-8.
59. Romanov YA, Svintsitskaya VA, Smirnov VN. Searching for alternative sources of postnatal human mesenchymal stem cells: candidate MSC-like cells from umbilical cord. *Stem Cells* 2003;21(1):105-10.
60. Wang Y, Chen X, Cao W, Shi Y. Plasticity of mesenchymal stem cells in immunomodulation: pathological and therapeutic implications. *Nat Immunol* 2014;15(11):1009-16.
61. Nagamura-Inoue T, He H. Umbilical cord-derived mesenchymal stem cells: Their advantages and potential clinical utility. *World J Stem Cells* 2014;6(2):195-202.

62. Krabbe C, Zimmer J, Meyer M. Neural transdifferentiation of mesenchymal stem cells--a critical review. *Apmis* 2005;113(11-12):831-44.
63. Scuteri A, Miloso M, Foudah D, et al. Mesenchymal stem cells neuronal differentiation ability: a real perspective for nervous system repair? *Curr Stem Cell Res Ther* 2011;6(2):82-92.
64. Kabos P, Ehtesham M, Kabosova A, Black KL, Yu JS. Generation of neural progenitor cells from whole adult bone marrow. *Exp Neurol* 2002;178(2):288-93.
65. Lindvall O, Kokaia Z, Martinez-Serrano A. Stem cell therapy for human neurodegenerative disorders-how to make it work. *Nat Med* 2004;10 Suppl:S42-50.
66. Zhang HT, Fan J, Cai YQ, et al. Human Wharton's jelly cells can be induced to differentiate into growth factor-secreting oligodendrocyte progenitor-like cells. *Differentiation* 2010;79(1):15-20.
67. Balasubramanian S, Thej C, Venugopal P, et al. Higher propensity of Wharton's jelly derived mesenchymal stromal cells towards neuronal lineage in comparison to those derived from adipose and bone marrow. *Cell Biol Int* 2013;37(5):507-15.
68. Karahuseyinoglu S, Cinar O, Kilic E, et al. Biology of stem cells in human umbilical cord stroma: in situ and in vitro surveys. *Stem Cells* 2007;25(2):319-31.
69. He H, Nagamura-Inoue T, Tsunoda H, et al. Stage-specific embryonic antigen 4 in Wharton's jelly-derived mesenchymal stem cells is not a marker for proliferation and

multipotency. *Tissue Eng Part A* 2014;20(7-8):1314-24.

70. Ishige I, Nagamura-Inoue T, Honda MJ, et al. Comparison of mesenchymal stem cells derived from arterial, venous, and Wharton's jelly explants of human umbilical cord. *Int J Hematol* 2009;90(2):261-9.

71. Ahn SY, Chang YS, Park WS. Mesenchymal stem cells transplantation for neuroprotection in preterm infants with severe intraventricular hemorrhage. *Korean J Pediatr* 2014;57(6):251-6.

72. Chen CW, Montelatici E, Crisan M, et al. Perivascular multi-lineage progenitor cells in human organs: regenerative units, cytokine sources or both? *Cytokine Growth Factor Rev* 2009;20(5-6):429-34.

73. Askarinam A, James AW, Zara JN, et al. Human perivascular stem cells show enhanced osteogenesis and vasculogenesis with Nel-like molecule I protein. *Tissue Eng Part A* 2013;19(11-12):1386-97.

74. Crisan M, Corselli M, Chen WC, Peault B. Perivascular cells for regenerative medicine. *J Cell Mol Med* 2012;16(12):2851-60.

75. Mori H, Ninomiya K, Kino-oka M, et al. Effect of neurosphere size on the growth rate of human neural stem/progenitor cells. *J Neurosci Res* 2006;84(8):1682-91.

76. Scholer HR, Ruppert S, Suzuki N, Chowdhury K, Gruss P. New type of POU domain in germ line-specific protein Oct-4. *Nature* 1990;344(6265):435-9.

77. Niwa H, Miyazaki J, Smith AG. Quantitative expression of Oct-3/4 defines differentiation, dedifferentiation or self-renewal of ES cells. *Nat Genet* 2000;24(4):372-6.
78. Mitsui K, Tokuzawa Y, Itoh H, et al. The homeoprotein Nanog is required for maintenance of pluripotency in mouse epiblast and ES cells. *Cell* 2003;113(5):631-42.
79. Hussain I, Magd SA, Eremin O, El-Sheemy M. New approach to isolate mesenchymal stem cell (MSC) from human umbilical cord blood. *Cell Biol Int* 2012;36(7):595-600.
80. Guo L, Zhou Y, Wang S, Wu Y. Epigenetic changes of mesenchymal stem cells in three-dimensional (3D) spheroids. *J Cell Mol Med* 2014;18(10):2009-19.
81. Ilieva M, Dufva M. SOX2 and OCT4 mRNA-expressing cells, detected by molecular beacons, localize to the center of neurospheres during differentiation. *PLoS One* 2013;8(8):e73669.
82. Pastrana E, Silva-Vargas V, Doetsch F. Eyes wide open: a critical review of sphere-formation as an assay for stem cells. *Cell Stem Cell* 2011;8(5):486-98.
83. Kuroda Y, Kitada M, Wakao S, et al. Unique multipotent cells in adult human mesenchymal cell populations. *Proc Natl Acad Sci U S A* 2010;107(19):8639-43.
84. Wakao S, Kuroda Y, Ogura F, Shigemoto T, Dezawa M. Regenerative Effects of Mesenchymal Stem Cells: Contribution of Muse Cells, a Novel Pluripotent Stem Cell Type that Resides in Mesenchymal Cells. *Cells* 2012;1(4):1045-60.

85. Lambert WS, Clark AF, Wordinger RJ. Neurotrophin and Trk expression by cells of the human lamina cribrosa following oxygen-glucose deprivation. *BMC Neurosci* 2004;5:51.
86. Deng C, Qin A, Zhao W, et al. Up-regulation of CXCR4 in rat umbilical mesenchymal stem cells induced by serum from rat with acute liver failure promotes stem cells migration to injured liver tissue. *Mol Cell Biochem* 2014;396(1-2):107-16.
87. Ruster B, Gottig S, Ludwig RJ, et al. Mesenchymal stem cells display coordinated rolling and adhesion behavior on endothelial cells. *Blood* 2006;108(12):3938-44.
88. Sturrock RR, Smart IH. A morphological study of the mouse subependymal layer from embryonic life to old age. *J Anat* 1980;130(Pt 2):391-415.
89. Clancy B, Darlington RB, Finlay BL. Translating developmental time across mammalian species. *Neuroscience* 2001;105(1):7-17.
90. van Velthoven CT, Kavelaars A, van Bel F, Heijnen CJ. Mesenchymal stem cell treatment after neonatal hypoxic-ischemic brain injury improves behavioral outcome and induces neuronal and oligodendrocyte regeneration. *Brain Behav Immun* 2010;24(3):387-93.
91. Liao W, Xie J, Zhong J, et al. Therapeutic effect of human umbilical cord multipotent mesenchymal stromal cells in a rat model of stroke. *Transplantation* 2009;87(3):350-9.
92. Liu AM, Lu G, Tsang KS, et al. Umbilical cord-derived mesenchymal stem cells with forced expression of hepatocyte growth factor enhance remyelination and functional recovery in a rat intracerebral hemorrhage model. *Neurosurgery* 2010;67(2):357-65; discussion 65-6.

93. van Velthoven CT, Braccioli L, Willemen HL, Kavelaars A, Heijnen CJ. Therapeutic potential of genetically modified mesenchymal stem cells after neonatal hypoxic-ischemic brain damage. *Mol Ther* 2014;22(3):645-54.
94. van Velthoven CT, van de Looij Y, Kavelaars A, et al. Mesenchymal stem cells restore cortical rewiring after neonatal ischemia in mice. *Ann Neurol* 2012;71(6):785-96.
95. Tillmann BU, Emons D, Bartmann P, Fahnenstich H. Posthemorrhagic unilateral hydrocephalus: fenestration of septum pellucidum as an alternative to shunt implantation. *J Pediatr* 2004;144(1):126-8.
96. Menet V, Prieto M, Privat A, Gimenez y Ribotta M. Axonal plasticity and functional recovery after spinal cord injury in mice deficient in both glial fibrillary acidic protein and vimentin genes. *Proc Natl Acad Sci U S A* 2003;100(15):8999-9004.
97. Wang Y, Gao Z, Zhang Y, et al. Attenuated Reactive Gliosis and Enhanced Functional Recovery Following Spinal Cord Injury in Null Mutant Mice of Platelet-Activating Factor Receptor. *Mol Neurobiol* 2016;53(5):3448-61.
98. Vinukonda G, Zia MT, Bhimavarapu BB, et al. Intraventricular hemorrhage induces deposition of proteoglycans in premature rabbits, but their in vivo degradation with chondroitinase does not restore myelination, ventricle size and neurological recovery. *Exp Neurol* 2013;247:630-44.
99. Dummula K, Vinukonda G, Chu P, et al. Bone morphogenetic protein inhibition

promotes neurological recovery after intraventricular hemorrhage. *J Neurosci* 2011;31(34):12068-82.

100. Poduslo JF, Curran GL. Permeability at the blood-brain and blood-nerve barriers of the neurotrophic factors: NGF, CNTF, NT-3, BDNF. *Brain Res Mol Brain Res* 1996;36(2):280-6.

101. Pan W, Yu Y, Yemane R, et al. Permeation of hepatocyte growth factor across the blood-brain barrier. *Exp Neurol* 2006;201(1):99-104.

102. Qi Z, Zhang H, Fu C, et al. Prolonged hydrocephalus induced by intraventricular hemorrhage in rats is reduced by curcumin therapy. *Neurosci Lett* 2017;637:120-5.

103. Guo ZY, Sun X, Xu XL, et al. Human umbilical cord mesenchymal stem cells promote peripheral nerve repair via paracrine mechanisms. *Neural Regen Res* 2015;10(4):651-8.

104. Peckham H, Giuffrida L, Wood R, et al. Fyn is an intermediate kinase that BDNF utilizes to promote oligodendrocyte myelination. *Glia* 2016;64(2):255-69.

105. Xiao J, Wong AW, Willingham MM, et al. Brain-derived neurotrophic factor promotes central nervous system myelination via a direct effect upon oligodendrocytes. *Neurosignals* 2010;18(3):186-202.

106. Yan H, Rivkees SA. Hepatocyte growth factor stimulates the proliferation and migration of oligodendrocyte precursor cells. *J Neurosci Res* 2002;69(5):597-606.

107. Kadoyama K, Funakoshi H, Ohya W, Nakamura T. Hepatocyte growth factor (HGF) attenuates gliosis and motoneuronal degeneration in the brainstem motor nuclei of a transgenic mouse model of ALS. *Neurosci Res* 2007;59(4):446-56.
108. Mukai T, Nagamura-Inoue T, Shimazu T, et al. Neurosphere formation enhances the neurogenic differentiation potential and migratory ability of umbilical cord-mesenchymal stromal cells. *Cytotherapy* 2015.
109. Bernardo ME, Zaffaroni N, Novara F, et al. Human bone marrow derived mesenchymal stem cells do not undergo transformation after long-term in vitro culture and do not exhibit telomere maintenance mechanisms. *Cancer Res* 2007;67(19):9142-9.
110. Luetzkendorf J, Nerger K, Hering J, et al. Cryopreservation does not alter main characteristics of Good Manufacturing Process-grade human multipotent mesenchymal stromal cells including immunomodulating potential and lack of malignant transformation. *Cytotherapy* 2015;17(2):186-98.
111. Tarte K, Gaillard J, Lataillade JJ, et al. Clinical-grade production of human mesenchymal stromal cells: occurrence of aneuploidy without transformation. *Blood* 2010;115(8):1549-53.
112. Nakamura T, Nishizawa T, Hagiya M, et al. Molecular cloning and expression of human hepatocyte growth factor. *Nature* 1989;342(6248):440-3.
113. Shang J, Deguchi K, Ohta Y, et al. Strong neurogenesis, angiogenesis,

synaptogenesis, and antifibrosis of hepatocyte growth factor in rats brain after transient middle cerebral artery occlusion. *J Neurosci Res* 2011;89(1):86-95.

114. Zeng W, Ju R, Mao M. Therapeutic potential of hepatocyte growth factor against cerebral ischemia (Review). *Exp Ther Med* 2015;9(2):283-8.

115. Liu XS, Li JF, Wang SS, et al. Human umbilical cord mesenchymal stem cells infected with adenovirus expressing HGF promote regeneration of damaged neuron cells in a Parkinson's disease model. *Biomed Res Int* 2014;2014:909657.

116. Kim D, Chung S, Lee SH, et al. Decreased hippocampal brain-derived neurotrophic factor and impaired cognitive function by hypoglossal nerve transection in rats. *J Cell Mol Med* 2017.

117. Lee J, Duan W, Mattson MP. Evidence that brain-derived neurotrophic factor is required for basal neurogenesis and mediates, in part, the enhancement of neurogenesis by dietary restriction in the hippocampus of adult mice. *J Neurochem* 2002;82(6):1367-75.

118. Pollock K, Dahlenburg H, Nelson H, et al. Human Mesenchymal Stem Cells Genetically Engineered to Overexpress Brain-derived Neurotrophic Factor Improve Outcomes in Huntington's Disease Mouse Models. *Mol Ther* 2016;24(5):965-77.

119. Reichardt LF. Neurotrophin-regulated signalling pathways. *Philos Trans R Soc Lond B Biol Sci* 2006;361(1473):1545-64.

120. Ma HC, Shi XL, Ren HZ, Yuan XW, Ding YT. Targeted migration of mesenchymal

stem cells modified with CXCR4 to acute failing liver improves liver regeneration. *World J Gastroenterol* 2014;20(40):14884-94.

121. Vinukonda G, Csiszar A, Hu F, et al. Neuroprotection in a rabbit model of intraventricular haemorrhage by cyclooxygenase-2, prostanoid receptor-1 or tumour necrosis factor-alpha inhibition. *Brain* 2010;133(Pt 8):2264-80.

## **IX. Acknowledgments**

First and foremost, I would like to express my sincere appreciation and gratitude to my supervisor Tokiko Nagamura-Inoue (Department of Cell Processing and Transfusion, The Institute of Medical Science, The University of Tokyo) and Arinobu Tojo (Division of Molecular of Therapy, Center for Advanced Medical Research, The Institute of Medical Science, The University of Tokyo) whose comments were of inestimable value for my study.

I would also like to thank the following collaborators: Yuka Mori, Atsuko Takahashi, Takahisa Shimazu (Department of Cell Processing and Transfusion, The Institute of Medical Science, The University of Tokyo), Shigeru Kiryu (Department of Radiology, The Institute of Medical Science, The University of Tokyo), Yasunori Ota and Haruo Onoda (Department of Pathology, The Institute of Medical Science, The University of Tokyo), and Muneyoshi Futami (Division of Molecular of Therapy, Center for Advanced Medical Research, The Institute of Medical Science, The University of Tokyo) for their technical assistance.

I would like to express my gratitude to Hajime Tsunoda (Department of Obstetrics, NTT Medical Center Tokyo Hospital), Satoru Yamaguchi (Department of Obstetrics, Yamaguchi Hospital) and the staff of NTT Medical Center Hospital and Yamaguchi Hospital, Tokyo, for their assistance with the collection of UC and CB. And this study was partially supported by the joint research study of The University of Tokyo with Rohto Pharmaceutical Co., Ltd. in the development of culture medium.